*minerals*

MDPI

*Article*

# Lamprophyre-Carbonatite Magma Mingling and Subsolidus Processes as Key Controls on Critical Element Concentration in Carbonatites—The Bonga Complex (Angola)

**Sandra Amores-Casals [1,2,*], Joan-Carles Melgarejo [1], Aurora Bambi [3], Antonio Olimpio Gonçalves [3], Eduardo Alves Morais [3], Jose Manuel [3], Andre Buta Neto [3], Alessandra Costanzo [4] and Joan Martí Molist [5]**

1 Departament de Mineralogia, Petrologia i Geologia Aplicada, Universitat de Barcelona, 08028 Catalunya, Spain; joan.carles.melgarejo.draper@ub.edu
2 Geomar Enginyeria del Terreny SLP, 08015 Barcelona, Spain
3 Departamento de Geologia, Faculdade de Ciências, Universidade Agostinho Neto, Luanda, Caixa Postal 815, Angola; aurorabambi@hotmail.com (A.B.); tonygoncalves72@hotmail.com (A.O.G.); mlmorais@netangola.com (E.A.M.); jomaplastov@hotmail.com (J.M.); anbuneto@hotmail.com (A.B.N.)
4 Earth and Ocean Sciences, National University of Ireland, SW4 794 Galway, Ireland; alessandra.costanzo@nuigalway.ie
5 Institut de Ciències de la Terra Jaume Almera, CSIC. 08028 Barcelona, Spain; joan.marti@ictja.csic.es
* Correspondence: sandra.amores.casals@gmail.com; Tel.: +34-625-099-009

Received: 22 July 2019; Accepted: 29 September 2019; Published: 30 September 2019


**Abstract:** The Bonga complex is composed of a central carbonatite plug (with a ferrocarbonatite core) surrounded by carbonatite cone sheets and igneous breccias of carbonatitic, fenitic, phoscoritic and lamprophyric xenoliths set in a carbonatitic, lamprophyric or mingled mesostase. To reconstruct the dynamics of the complex, the pyrochlore composition and distribution have been used as a proxy of magmatic-hydrothermal evolution of the complex. An early Na-, F-rich pyrochlore is disseminated throughout the carbonatite plug and in some concentric dykes. Crystal accumulation led to enrichment of pyrochlore crystals in the plug margins, phoscoritic units producing high-grade concentric dykes. Degassing of the carbonatite magma and fenitization reduced F and Na activity, leading to the crystallization of magmatic Na-, F- poor pyrochlore but progressively enriched in LILE and HFSE. Mingling of lamprophyric and carbonatite magmas produced explosive processes and the formation of carbonatite breccia. Pyrochlore is the main Nb carrier in mingled carbonatites and phoscorites, whereas Nb is concentrated in perovskite within mingled lamprophyres. During subsolidus processes, hydrothermal fluids produced dolomitization, ankeritization and silicification. At least three pyrochlore generations are associated with late processes, progressively enriched in HFSE, LILE and REE. In the lamprophyric units, perovskite is replaced by secondary Nb-rich perovskite and Nb-rich rutile. REE-bearing carbonates and phosphates formed only in subsolidus stages, along with late quartz; they may have been deposited due to the release of the REE from magmatic carbonates during the hydrothermal processes.

**Keywords:** Nb; pyrochlore; perovskite; zirconolite; carbonatite; aillikite; alnöite; REE carbonates and phosphates; magma mingling; subsolidus processes

## 1. Introduction

Carbonatites s.s. are mantle-derived, igneous rocks made up of more than 50% primary carbonate, normally produced in cratonic domains affected by rifting or, rarely, on some oceanic island [1].

Hence, this definition should exclude crustal "anatectic carbonatites" found in some mobile belts [2]. Carbonatites worldwide [1,3] are important carriers for critical raw materials such as Nb, REE, fluorite and phosphate but also of Cu, Mo, Fe, barite, both in the primary rocks [4–49] or in the weathered carapace [50–52]. One of the main problems related to the exploration and exploitation of these elements is still the poor understanding of the crystallization processes in carbonatites. Carbonatite magmas crystallize in plutonic, hypabyssal and volcanic domains with therefore different crystallization processes, including in some cases explosive processes. The existence of large-scale hydrothermal replacements, also leading to the development of mineralization, has been documented either in the host rock (fenitization) [53–55] or in the carbonatite itself [56–58]. This implies that it is not always simple to determine the importance of the hydrothermal (or carbothermal) overprint of the primary associations. Textural and isotope studies suggest that hydrothermalism overprinted the mineral associations in different grades in many occurrences [59] and that, therefore, it may affect the distribution of critical metals. In addition, carbonatites are generally associated with alkaline undersaturated rocks [60] and ultramafic lamprophyres [61–64] and a classical problem is the petrogenetic link between these rocks, although some mingling processes among these magmas have been described [65]. The metallogenetic potential of these associated rocks and its influence on the enrichment of critical elements in the carbonatites are still poorly known.

The Angolan carbonatite occurrences often form ring complexes and carbonatite intrusions, most of them associated with undersaturated alkaline rocks or lamprophyres and set in three emplacement levels—plutonic (Tchivira [66–68]; Monte Verde [69,70]), hypabyssal (Bonga [67,68,70]; Virulundo [71]) and extrusive (Catanda; [67,68,72]). The intrusions often constitute ring complexes of carbonatite, most of them associated with alkaline rocks [66–72]. Some of these carbonatite occurrences are among the largest in the world and are mineralized in fluorite [73], iron and pyrochlore [74], with many mining exploration operations currently in process. Pyrochlore chemistry, often used as proxy of magmatic and subsolidus processes, has been used to define the carbonatite evolution [66,67,69,71].

The Bonga complex is one of the largest carbonatitic outcrops in Angola and worldwide [75], with well-known resources in pyrochlore [68,76]. Existing studies focus on the general pyrochlore composition in the carbonatites but there is no information about other minerals also rich in critical elements or on the behaviour of pyrochlore and of these minerals within the different rocks of the complex. For this reason, the objective of this contribution is to show the distribution of these minerals among the different lithotypes (ultramafic lamprophyres and carbonatite facies) of the Bonga complex. This complex is a good representative case of a system integrating different rock types associated with carbonatitic magmatism. In order to establish the distribution of Nb and REE minerals, a detailed petrographic characterization and mineral chemistry study of the Nb and REE rich minerals is presented. We focus on rocks with the highest concentrations of Nb and REE and the processes (magmatic and hydrothermal) by which they accumulate.

## 2. Geological Setting

The Bonga carbonatite, located SE of Quilengues, Huila Province, Angola (Figure 1), is a carbonatite-alkaline complex related to the Lucapa graben, a megastructure cutting Congo, Kasai and Angola Cratons and reactivated during the opening of the South Atlantic Ocean in Early Cretaceous [77,78]. This magmatism has counterparts at the other side of the Atlantic, forming part of the Parana-Angola-Namibia alkaline province [78–80]. The Lucapa extensional stage provided conduits for carbonatite, alkaline and kimberlite magmas rising from the mantle. Kimberlite occurrences are concentrated at the north-eastern part of the graben whereas carbonatites and their associated alkaline rocks are located in the southwestern and central domains [3]. Recent dating analyses confirm that kimberlite (for instance, Catoca, 117 ± 0.7 My; Tchiuzo, 121.2 ± 1 My; Mulepe 1, 116.2 ± 6.5, Mulepe 2, 123.0 ± 3.6 My, Calonda, 119.5 ± 4.3 My, Cat115, 133 ± 10 My [81–83]), alkaline rocks (Tchivira nepheline syenites, 112 ± 8 My, 130.8 ± 1.4 My and 130 ± 13.8 My [84]) and ultramafic lamprophyres (Bonga alnöite, 133.9 ± 5.5 My, 136.9 ± 5.6 My [70]) intruded in the Lucapa structure during the Early

Cretaceous and having all magmas formed at the same event. However, carbonatite lavas of the Catanda carbonatite (Kwanza Sul, Central Angola) reveal ages of ~0.5 Ma [85,86] implying recent extensional events in some areas of the Lucapa graben.

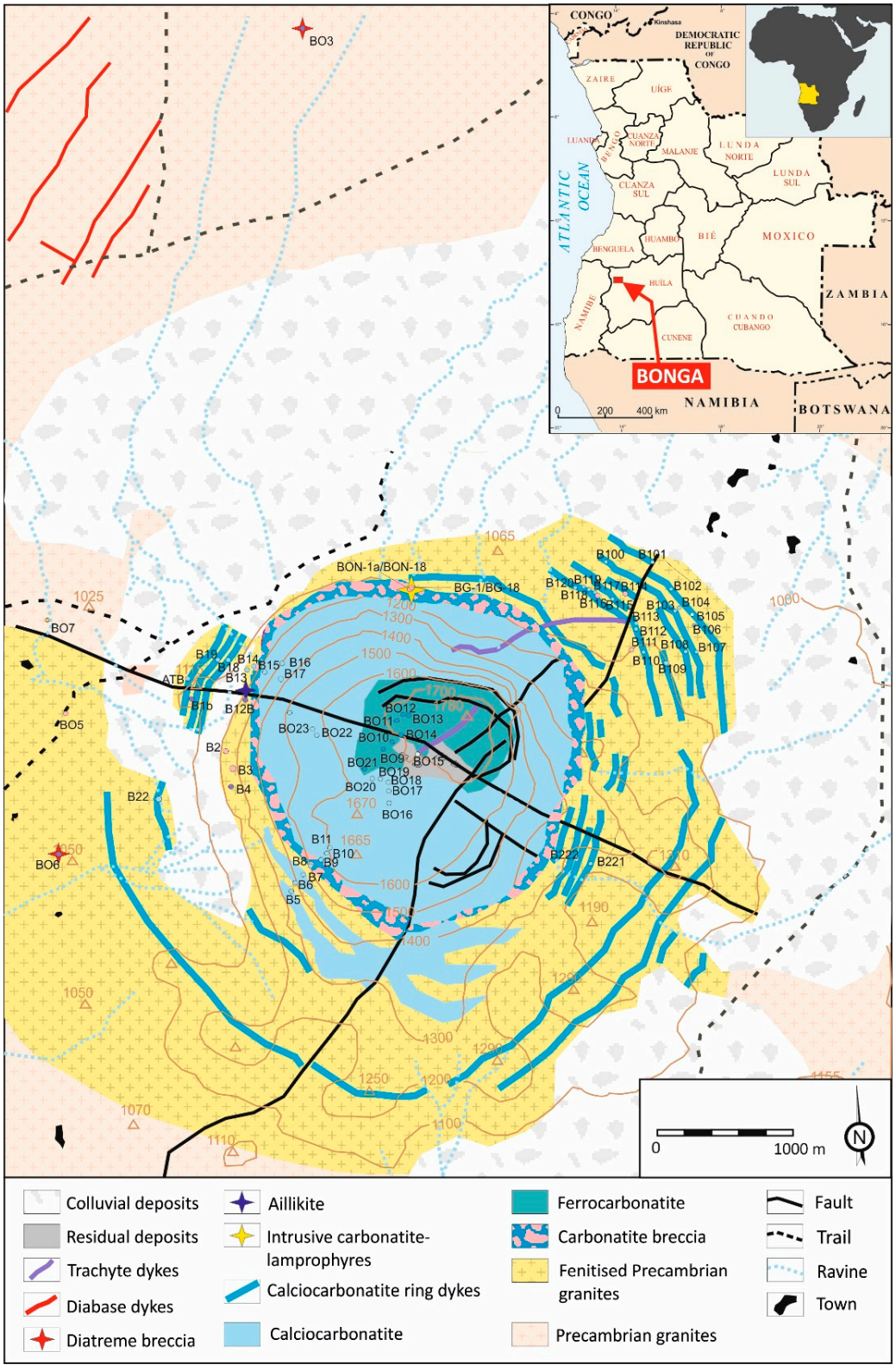


**Figure 1.** Geological map of units composing the Bonga complex, with the location of the field samples. Modified from Lapido–Loureiro [75] and Bambi [68].

The Bonga intrusion forms a polygenetic complex with the plutonic Tchivira complex located 10 km southwest [68,70]. Bonga corresponds to a more superficial level than Tchivira.

## 3. Materials and Methods

Samples were collected during several field trips in Angola. 130 polished thin sections were analysed in order to identify mineral phases and investigate textural features using transmitted-reflected optical microscopy with plane and crossed polarized light. The most representative areas were then selected to be studied by SEM-EDS. Qualitative analyses and detailed characterization of zoning patterns were carried out using a ESEM Quanta Q-200 FEI XTE 325/D8395 Scanning Electron Microscope (Thermo Fisher Scientific, Waltham, MA, USA) coupled with a INCA Energy 250 EDS microanalysis system, located at the Scientific and Technological Centers of the University of Barcelona. Operating conditions were 20 keV and 1 nA beam current and 10 mm between sample and detector. 12 samples were selected in order to quantify pyrochlore types and zoning trends using a JEOL JXA-8230 electron microprobe (JEOL USA, Peabody, MA, USA) with five wavelength dispersive spectrometers (JEOL USA, Peabody, MA, USA), also located at the Scientific and Technological Centers of the Unversity of Barcelona. Operating conditions were 20 keV and 14.4 nA.

The calibration standards and lines used for pyrochlore and perovskite were—$UO_2$ (U, $M\beta$, PETJ), orthoclase (K, $K\alpha$, PETJ), $ThO_2$ (Th, $M\alpha$, PETJ), rutile (Ti, $K\alpha$, PETJ), LaB6 (La, $L\alpha$, PETJ), $CeO_2$ (Ce, $L\alpha$, PETJ), corundum (Al, $K\alpha$, TAPH), periclase (Mg, $K\alpha$, TAPH), albite (Na, $K\alpha$, TAPH), wollastonite (Si, $K\alpha$, TAPH), fluorite (F, $K\alpha$, TAPH), barite (Ba, $L\alpha$, LIFH), $REE^{-4}$ (Nd, $L\beta$, LIFH), rhodonite (Mn, $K\alpha$, LIFH), $REE^{-3}$ (Sm, $L\beta$, LIFH), $Fe_2O_3$ (Fe, $K\alpha$, LIFH), Ta (Ta, $L\alpha$, LIFH), wollastonite (Ca, $K\alpha$, PETL), PbS (Pb, $M\alpha$, PETL), Nb (Nb, $L\alpha$, PETL), $ZrO_2$ (Zr, $L\alpha$, PETL) and celestine (Sr, $L\alpha$, PETL). Standards and lines used for zircon, zirconolite and baddeleyite are the same as for pyrochlore but adding $ZrSiO_4$ (Zr, $L\alpha$, PETL), Hf (Hf, $L\beta$, LIFH) and YAG (Y, $L\alpha$, PETL).

## 4. The Structure and Lithology of the Alkaline–Lamprophyre–Carbonatite Bonga Complex

The Bonga complex has a concentrically zoned structure (Figure 1). The core of the complex is a massive almost circular carbonatite plug, up to 2 km in diameter and about 1000 m in height. It is composed mainly of banded or massive calciocarbonatites. Banding is defined by the enrichment in accessory minerals (apatite, magnetite, phlogopite and richterite). Ankerite, along with the above-mentioned accessory minerals, is the dominant mineral in the core of the plug. This area has been strongly affected by karstification processes and intense weathering; therefore, the primary textures are not preserved and ankerite is strongly replaced by mixtures of goethite and secondary calcite. For this reason, it is difficult to determine if this ankerite is primary magmatic or produced by hydrothermal replacement. Pyrochlore is fluorcalciopyrochlore in composition in the unaltered carbonatite but it may be variably replaced by secondary generations of pyrochlore in hydrothermally altered domains [67,68,76]. It forms euhedral to subhedral crystals (up to 500 μm) scattered in the carbonatite groundmass.

This carbonatite plug is rimmed by a subvertical carbonatitic magmatic breccia up to 100 m wide. The groundmass of these magmatic breccias is generally carbonatitic but may be locally extremely heterogeneous and include complex mixtures of carbonatitic and lamproitic spherical bodies. In addition, these rocks have been affected by subsolidus processes. Therefore, these mixed units (described in this work as Intrusive Mixed Carbonatite-Lamprophyre complex, IMCL) will be described in detail because their complex mineralization allows examination of the Nb minerals distribution's among carbonatitic and lamprophyric units. Other rare magmatic breccias with carbonatitic groundmass occur as discrete small diatremes (20–50 m in diameter) in the proximities of the complex, 3 km north or 1 km west of the plug (Figure 1). These intrusions do not contain mineralization.

The outer units comprise successive massive calciocarbonatite concentric dykes, 10 to 100 m wide. These dykes dip between 50–75° towards the plug and are therefore interpreted as cone sheets. Many of these dykes have an analogous mineralogy and texture with the carbonatites of the central plug but others are highly enriched in accessory minerals and a clear positive correlation between the

pyrochlore content and the proportions of other accessory minerals, that is, apatite and magnetite, has been established in these rocks [67,68,76]. Moreover, pyrochlore crystals can reach up to 1 cm in length and are often intergrown with apatite, magnetite, phlogopite and richterite.

Late trachyte dykes cut the central units and basaltic dykes trending NE–SW were emplaced in the vicinity of the complex; these volcanic rocks do not contain rare-element mineralization. All the above units are hosted by highly fenitized Eburnean granites. Pyrochlore and REE minerals are very rare in these fenites.

Extensive colluvial deposits are present at the base of the calciocarbonatite plug escarpments. Dense minerals such as magnetite, pyrochlore, apatite or barite are concentrated there by weathering of the lateritic products, whereas carbonate minerals are dissolved.

## 5. Nb and REE Distribution at the Intrusive Mixed Carbonatite-Lamprophyre Complex (IMCL)

The Intrusive Mixed Carbonatite-Lamprophyre (ICML) complex is a local heterogeneous unit composed by angular xenoliths of variable composition cemented by an interstitial groundmass of calciocarbonatite (Figure 2), aillikite or a mixture of both. It has a very irregular shape and their size, difficult to calculate because of dangerous access to the outcrops, can be estimated as more than 100 m width.

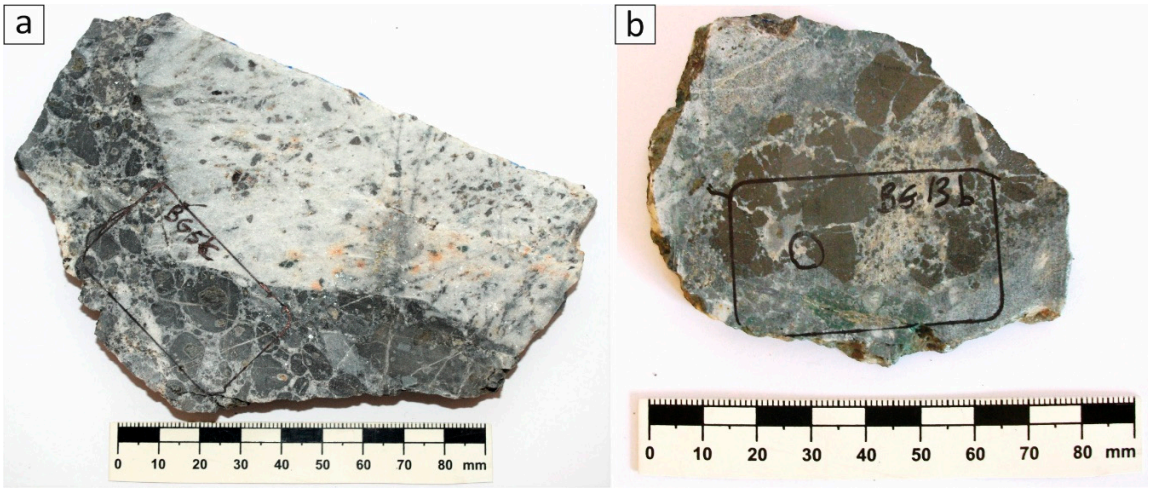


**Figure 2.** (**a**) Calciocarbonatite xenolith and sub-spherical aillikite bodies set in a calciocarbonatite groundmass; (**b**) apatite-magnetite phoscoritic xenoliths replaced and surrounded by fine calciocarbonatite groundmass.

The carbonatite groundmass contain aillikite spheroids (0.5–2 cm in diameter) and five types of irregular xenoliths—magnetite-apatite phoscorites, calciocarbonatites, magnesian xenoliths, olivine phoscorites and natrocarbonatites (Figure 3A). REE carbonates and REE phosphates, zirconolite and up to five generations of pyrochlore have an unequal distribution among these units.

Domains with aillikite groundmass contain alnöite spheroids and three types of irregular xenoliths—calciocarbonatite, turjaite and phlogopite-apatite-augite rocks (Figure 3B). These lamprophyres do not present neither pyrochlore nor REE minerals but accessory amounts of Nb-rich perovskite, zirconolite and Nb-rich phlogopite.

### *5.1. IMCL Domains with Carbonatite Groundmass*

#### 5.1.1. Carbonatite Groundmass

Major calcite and lesser amounts of primary apatite, magnetite, phlogopite and pyrochlore make up the carbonatite groundmass. Pervasive subsolidus processes (dolomitization, ankeritization and silicification) cause replacement of the previous minerals extensively. A significant Nb and REE

mineralization is represented by late pyrochlore generations, zircon, zirconolite, REE fluorocarbonates and REE phosphates in these replaced units.

Pyrochlore is a minor component (less than 2 modal %) and up to five generations of this mineral are identified. Euhedral primary pyrochlore crystals (named as type I) are intergrown with primary calcite, apatite and magnetite; they have concentric compositional zoning. This generation may form skeletal textures among primary magmatic calcite and apatite, thus suggesting a cocrystallization of pyrochlore with these minerals and a fast growth; zirconolite may be produced during the last stages of pyrochlore growth, along with magnetite (Figure 3A).

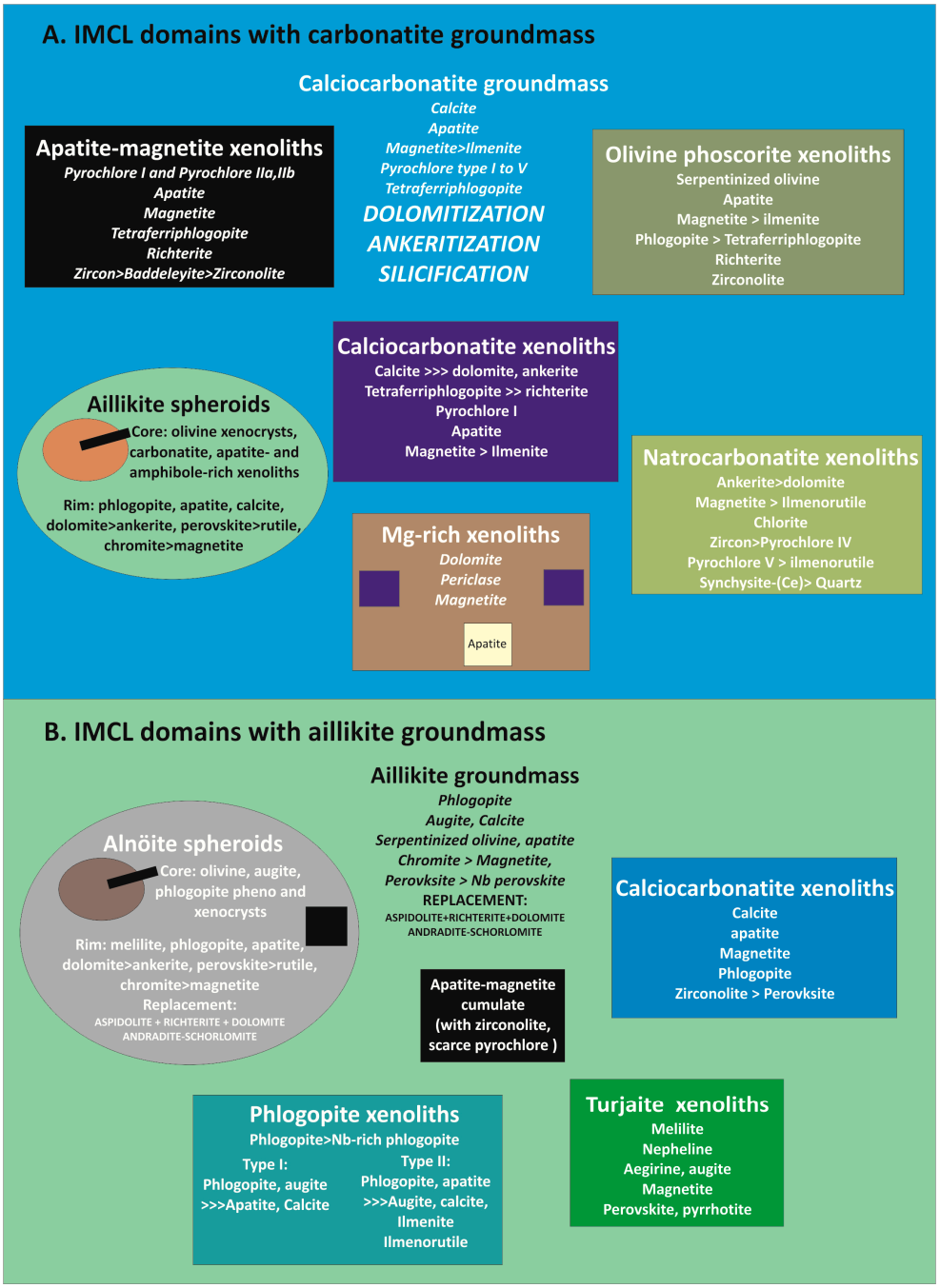


**Figure 3.** (**A**) Schematic diagram of ICML bodies of carbonatite groundmass—aillikite spheroids and xenoliths of calciocarbonatite, natrocarbonatite, olivine phoscorite, apatite-magnetite and Mg-rich rocks; (**B**) ICML bodies of aillikite groundmass—alnöite spheroids and xenoliths of calciocarbonatite, turjaite and phlogopite-rich.

Four successive generations of pyrochlore replace the primary one. Type II pyrochlore is associated with early stages of dolomitization usually as irregular overgrowths replacing the primary generations. A thin rim of type III pyrochlore (Figure 4b) may surround few type II pyrochlore crystals in these dolomitized areas. Pyrochlore IV has been found as irregular crystals in dolomitized or ankeritized areas or veins in the above mentioned pyrochlore generations and these crystals are associated with thorutite and uranothorianite (Figure 4c). At last, pyrochlore V grows in highly ankeritized and silicified domains, mainly as veins in the rest of the pyrochlore generations (Figure 4d) and filling geode cavities over saddle ankerite.

Zr minerals such as zircon or zirconolite found in the groundmass could correspond to xenocrysts deriving from disaggregation of apatite-magnetite xenoliths. However, zircon may also form in drusy cavities or replaces baddeleyite along with quartz, thus indicating a very late formation (Figure 4e).

REE carbonates are associated with quartz replacements and are scarce. Parisite-(Ce) forms fine anhedral crystals less than 10 microns in diameter, along with ilmenorutile and synchysite-(Ce). Tiny radial aggregates of synchysite-(Ce) (Figure 4f) occur in ankerite, also associated with late quartz. REE phosphates are less abundant. Rhabdophane-(Ce) forms botryoidal aggregates of fine radial fibres up to 10 microns associated to late quartz replacing apatite, calcite, ankerite and dolomite (Figure 4d).

#### 5.1.2. Carbonatite Xenoliths

Angular fragments of white calcite carbonatite are common in the breccia. Their size is variable but normally in the centimetric order. They have a phaneritic equigranular texture, with a grain size that may reach 1 cm. Calcite is more than 95% of the modal content and is accompanied by minor amounts of other minerals such as apatite, magnetite and at least two generations of pyrochlore (Figure 5a). The second generation of pyrochlore may overgrow or vein the first one. All these accessory minerals tend to be euhedral to subhedral.

#### 5.1.3. Apatite–Magnetite Xenoliths

Apatite-magnetite xenoliths present phaneritic equigranular texture formed by equal amounts of magnetite and apatite with lesser pyrochlore, zircon, phlogopite-tetraferriphlogopite and richteritic amphibole. Grain size tends to be about 1 cm in diameter. Calciocarbonatite groundmass invades the unit, partly filling fractures and as patches, often with secondary dolomite and ankerite.

Pyrochlore forms the same five generations described in the carbonatite groundmass. Type I pyrochlore occurs as subidiomorphic crystals from 50 μm to 0.5 mm long in equilibrium with apatite, tetraferriphlogopite and richterite. Four types of subsolidus pyrochlore appear distributed in veinlets and patches, as observed in carbonatite groundmass but in smaller proportions—type II and type III grow in dolomitized areas; type IV is associated with late dolomite, ankerite and strontianite; type V and late quartz are very scarce.

During late stages of ankeritization, zirconolite may precipitate overgrowing primary pyrochlore with both replacing primary zircon, displaying complex intergrowth textures (Figure 5b). During late stages, fine-grained aggregates of ilmenorutile and lucasite-(Ce) replace ilmenite and magnetite.

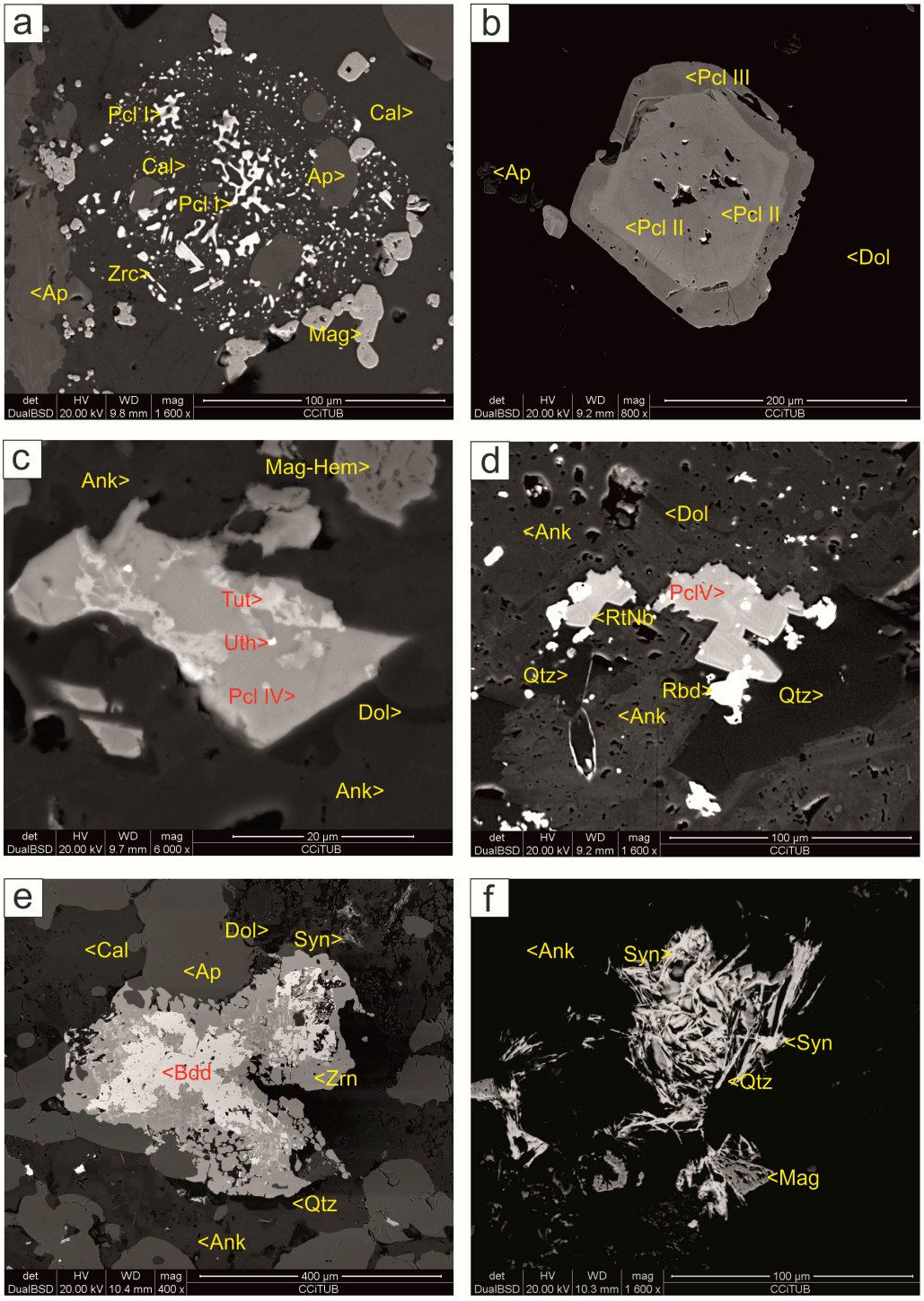


**Figure 4.** Nb- and REE- minerals in the carbonatite groundmass of the ICML breccias. SEM images, BSE mode. (**a**) BG-6l. Skeletal primary pyrochlore (Pcl I) intergrown with calcite (Cal) and apatite (Ap), partly overgrown by zirconolite (Zrc) and magnetite (Mag). (**b**) BG-6g. Euhedral magmatic type II crystals replaced by type III pyrochlore (Pcl II, Pcl III) among late dolomite (Dol) and apatite; (**c**) BG-6c. Type IV pyrochlore, replaced by uranothorianite (Uth) and thorutite (Tut), filling porosity in a dolomitized and ankeritized domain of the carbonatite groundmass. (**d**) BG-9c. Sequence of geode filling in altered groundmass—zoned euhedral ankerite is overgrown by late pyrochlore (Pcl V) followed by zoned ilmenorutile (RtNb), rhabdophane-(Ce) (Rbd) and finally quartz (Qtz); (**e**) BG-6o. Calcite replaced by dolomite, ankerite and quartz with synchysite-(Ce) (Syn) and zircon (Zrn) replacing baddeleyite (Bdd); (**f**) BG-7a. Fine aggregate of acicular synchysite among ankerite, quartz and magnetite (Mag).

#### 5.1.4. Spheroidal Aillikite Inclusions

Rounded inclusions of aillikite are abundant in the calciocarbonatite groundmass. These inclusions usually present concentric structure and heterogeneous composition. Carbonatite angular xenoliths, amphibole or olivine xenocrysts partly serpentinized and apatite-amphibole xenoliths constitutes the inner core; this core is surrounded by an external rim of fine-grained intergrowths of phlogopite, chromite rimmed by magnetite, perovskite and apatite. A late subsolidus association formed by dolomite, ankerite, quartz, strontianite and REE carbonates strongly replaces the outer zone of the aillikite spheroids in most of the cases.

Parisite-(Ce) and synchysite-(Ce) occur as fine radial aggregates or plates (Figure 5c) whereas REE phosphates are not present. Regarding Nb phases, only one crystal of type I pyrochlore was found in the external rim, suggesting that it could be part of the carbonatite groundmass, which is corroding the spheroids.

#### 5.1.5. Magnesian Xenoliths

Some scarce xenoliths consist of calcite with periclase; the latter is partially replaced by brucite and magnetite, accompanied by spherules of sellaite, spinel and portlandite. Radial aggregates of fine synchysite-(Ce) replace primary apatite. Primary pyrochlore is rare (pyrochlore I); it is partially replaced by a late Sr-rich pyrochlore generation (pyrochlore II) and overgrown by vigezzite, aeschynite and hydropyrochlore (Figure 5d).

#### 5.1.6. Natrocarbonatite Xenoliths

These are very scarce tabular crystals resembling the alkaline carbonate nyerereite. However, these crystals are fully pseudomorphized by fine-grained late ankerite. The rest of the original mineral association is also strongly replaced—ilmenorutile overgrows magnetite; dolomite, ankerite and quartz pseudomorphize chloritized phlogopite.

Primary calzirtite pseudomorphized by zircon and replaced by type IV pyrochlore, is commonly disseminated in this ankeritized rock. Type V pyrochlore, ilmenorutile and scarce synchysite-(Ce) in association with latest quartz replace the ensemble (Figure 5e).

#### 5.1.7. Olivine Phoscorite Xenoliths

Unlike the apatite-magnetite phoscoritic xenoliths, the phoscorite xenoliths contain major apatite, magnetite, ilmenite and serpentinized olivine with trace amounts of phlogopite-tetraferriphlogopite, calcite and richterite but do not present pyrochlore. Alternatively, they have zoned zirconolite, which displays patchy zoning owing to variations in the Nb, U and Th proportions. Zircon occurs in late associations, replacing zirconolite along with quartz. Magnetite, ilmenite and zirconolite are further altered to Ti-rich hydrous minerals such as lucasite-(Ce) and kassite, which form secondary fine radial aggregates in their rims (Figure 5f).

### *5.2. IMCL Domains with Aillikite Groundmass*

The IMCL domains with aillikite groundmass host xenoliths of turjaite, calciocarbonatite and phlogopite-apatite-augite; they also contain abundant centimetric-sized alnöite spherical bodies.

#### 5.2.1. Aillikite Groundmass

The aillikite groundmass (Figure 6a) of these domains is made up by major fine phlogopite laths, zoned diopside-augite included in anhedral poikilitic calcite, serpentinized olivine, with minor apatite, chromite overgrown by magnetite and Type I perovskite weakly zoned by Nb-rims (Type II perovskite). Locally, the following subsolidus minerals replaced the primary associations—late rutile, andradite-schorlomite and a late Na-rich alteration by aspidolite and richterite plus dolomite.

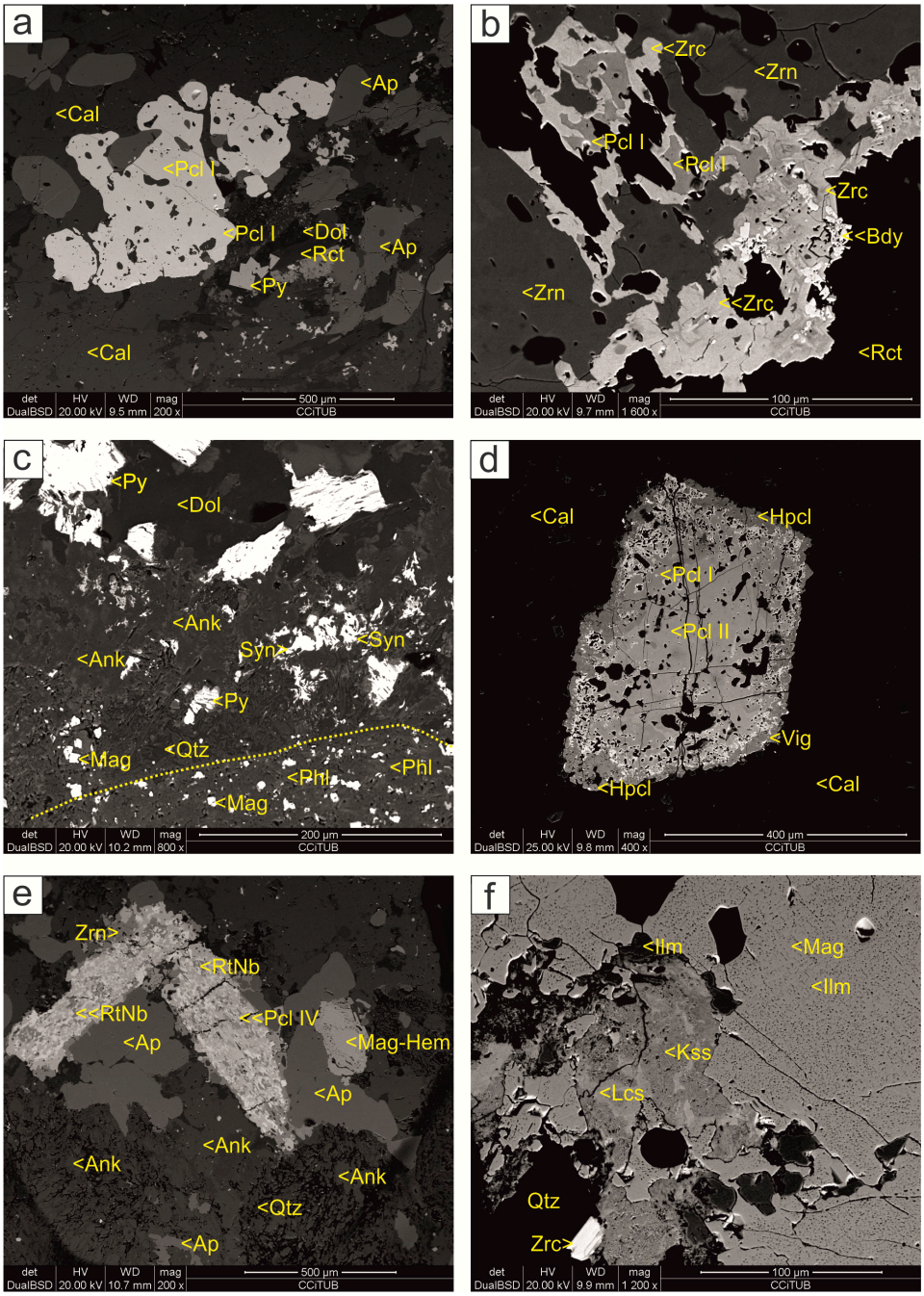


**Figure 5.** Nb and REE minerals at IMCL bodies cemented by carbonatite groundmass. SEM BSE images, BSE mode. (**a**) BG-5b. Calciocarbonatite xenolith. Pyrochlore type I (Pcl) intergrown with apatite (Ap) and calcite (Cal). Secondary dolomite (Dol), richterite (Rct) and pyrite (Py) replacing the ensemble. (**b**) BG-6k. Apatite-magnetite xenoliths. Pyrochlore I (PclI) and zircon (Zrn) replaced by zirconolite (Zrc) and finally by baddeleyite (Bdy); (**c**) BG-6j. Aillikite spheroid. Inner rim with synchysite-(Ce) (Syn) associated to late quartz (Qtz), ankerite (Ank) and pyrite (Py), all replacing dolomite (Dol). Outer rim is formed by fine magnetite (Mag) and phlogopite (Phl); (**d**) BG-14b. Mg-rich carbonatite xenolith. Pyrochlore I overgrown by pyrochlore II and both replaced by pyrochlore IV (Hpcl) and vigezzite (Vig); (**e**) BG-6r. Natrocarbonatite xenolith. A primary crystal (calzirtite?) pseudomorphosed by fine-graMained intergrowths of zircon (Zrn), quartz (Qtz), ilmenorutile (RtNb) and late pyrochlore (Pcl IV) among apatite (Ap), ankerite and magnetite replaced by hematite (Mag-Hem); (**f**) BG-6m. Phoscorite. Magnetite with ilmenite inclusions (Ilm) replaced by lucasite-(Ce) (Lcs) and kassite (Kss) aggregates. Zirconolite (Zrc) is associated to a stage of quartz replacement.

The most striking features in terms of hosts for rare elements are the occurrence of apatite-magnetite cumulates with scarce pyrochlore, along with significant baddeleyite and zirconolite (Figure 6b) and the absence of REE minerals.

#### 5.2.2. Turjaite Xenoliths

Some very rare xenoliths are made up by dominant melilite (more than 50 modal %), accessory but abundant (less than 25 modal %) nepheline and aegirine with trace magnetite and perovskite. According to their composition, these melilitolite xenoliths correspond to a turjaite [87]. Most of the crystals are extremely fine-grained (less than 10 microns in diameter). Perovskite occurs as individual microphenocrysts (Figure 6c). They may also overgrow magnetite or form skeletal intergrowths along with nepheline, augite, melilite and pyrrhotite.

#### 5.2.3. Calciocarbonatite Xenoliths

Calciocarbonatite xenoliths (1–5 cm in size) scattered among the aillikite groundmass show similarities with the carbonatite of the main plug, being made up by calcite, with accessory amounts of apatite, magnetite, phlogopite and pyrite. Zirconolite and perovskite are the major Nb carriers, because pyrochlore is extremely scarce. Zirconolite may form zoned subhedral crystals with variable Nb, Ta, Zr, Ti, U and Th locally replacing early calzirtite.

#### 5.2.4. Phlogopite-Rich Xenoliths

These are rare and consist of phlogopite dominant xenoliths, with lower proportions of augite and apatite. These rocks show a phaneritic texture and medium grain size. Two subgroups are identified—the first type presents a strong aillikitic affinity, as it contains zoned phlogopite and augite, lesser interstitial apatite and calcite. However, the second type shows apatite and phlogopite as major constituents having also less augite, calcite and accessory Nb-rich ilmenite overgrown by ilmenorutile. In both types, phlogopite displays a striking oscillatory zoning pattern giving irregular and curved bands of variable Al, Fe and Si contents and Nb enrichments in external rims but also in inner cores (Figure 6d).

#### 5.2.5. Alnöite Spheroids

Spherical to ellipsoidal alnöite inclusions are 1–4 cm in diameter. They show porphyritic texture defined by macrocrysts and xenocrysts of olivine, phlogopite and titanian augite set in an aphanitic groundmass. The alnöite groundmass differs from that of aillikite because the first contains major melilite laths (up to 100 μm in length), along with phlogopite, chromite (mantled by magnetite), primary perovskite (Type I) and apatite, whereas calcite is extremely scarce (Figure 6e).

Cores of perovskite crystals are Nb-poor (Type II perovskite) but the very fine rims are enriched in Nb. In addition, enrichments of apatite-magnetite-calcite are observed. Type I and II perovskite are replaced by late magnetite (Figure 6f) and the ensemble is replaced by symplectitic intergrowths of Na- and Nb-rich perovskite (Type III generation) and IV perovskite which shows LREE enrichments; zirconolite could replace magnetite.

## 6. Mineral Chemistry of Nb Minerals of the IMCL Bodies

Pyrochlore is the major carrier of Nb in the IMCL bodies of the Bonga complex. Up to five generations have been identified in the ICML domains of carbonatite groundmass (Figures 7 and 8). Pyrochlore types present compositions which may differ from the generations previously defined in other studies of the Bonga carbonatites carried out on the plug or the concentric dykes [67,68,88]. Nb also accumulates inside perovskite, baddeleyite, zircon, ilmenorutile and appear rarely concentrated in the phlogopite crystals from the phlogopite-rich xenoliths. Chemical analyses of Nb and REE minerals are available in the Supplementary Material section.

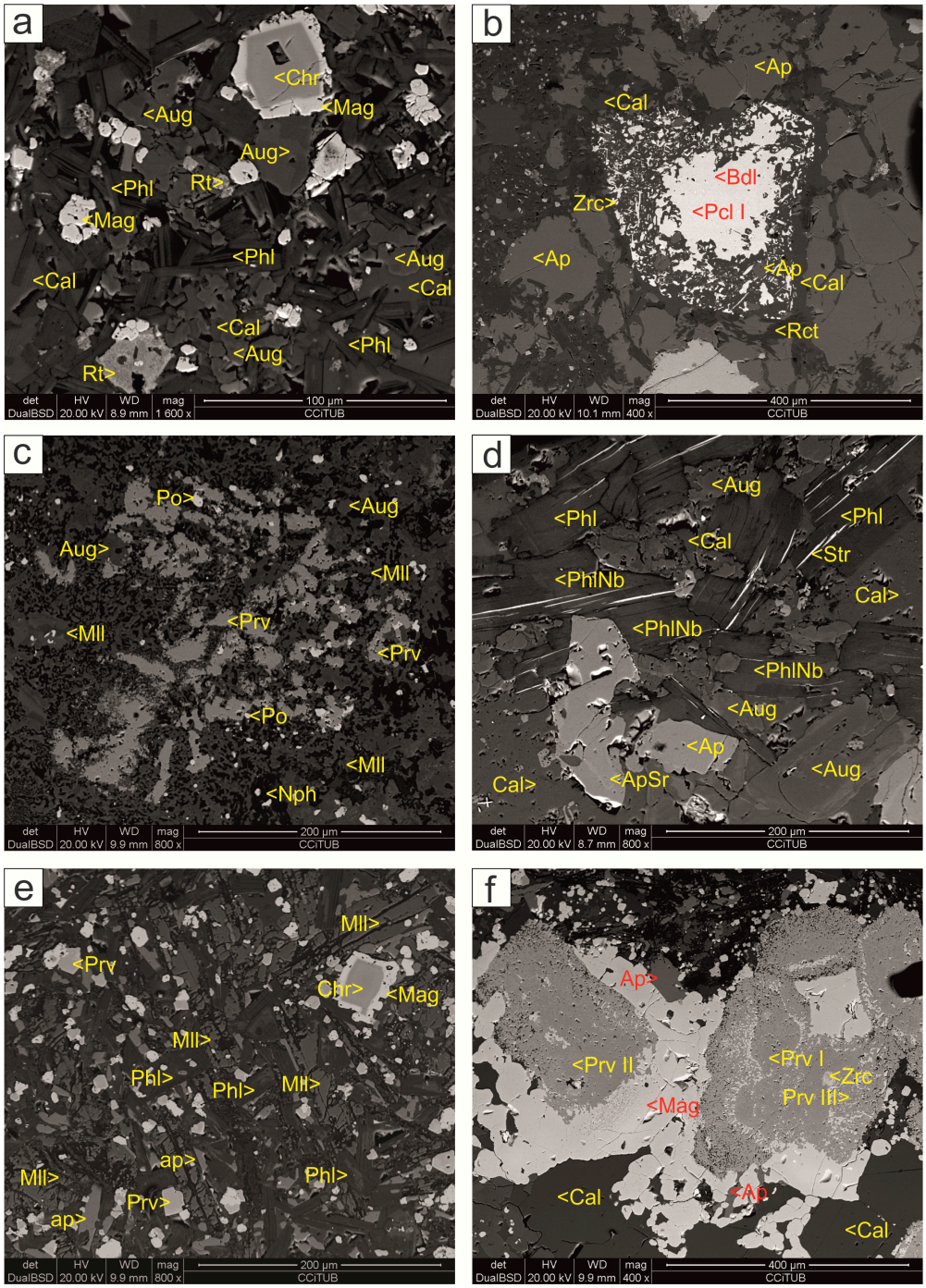


**Figure 6.** Nb and REE phases at the aillikite groundmass, turjaite, calciocarbonatite and phlogopite-rich xenoliths as well as alnöite spheroids. SEM BSE images, BSE mode. (**a**) BG-10a. Aillikite groundmass composed by zoned phlogopite (Phl), calcite (Cal), zoned augite (Aug), chromite (Chr) with magnetite rims (Mag) and rutile (Rt) replacing early perovskite; (**b**) BG-6b. Magmatic pyrochlore (Pcl I) with baddeleyite inclusions intergrown with apatite (Ap), calcite and zirconolite (Zrc). Apatite is associated with richterite (Rct); (**c**) BG-3a. Intergrowth of perovskite, Nb perovskite (Prv II), augite, nepheline (Nph) and melilite (Mll), with scattered pyrrhotite (Po); (**d**) BG-10a. Phlogopite-rich xenoliths. Zoned apatite, zoned augite, zoned phlogopite (variable Fe, Nb contents), strontianite (Str) filling phlogopite cleavages, calcite and fine augite. (**e**) BG-4a. Alnöite groundmass formed by melilite, perovskite (Prv I) with Nb rim (Prv II), phlogopite, apatite and chromite with magnetite rims; (**f**) BG-4a. Magnetite-apatite in alnöite groundmass. Nb and Na rich perovskite (types II and III) and zirconolite (Zrc) are pseudomorphosing magnetite and older perovskite generations (I and II).

### *6.1. Pyrochlore*

#### 6.1.1. Type I Pyrochlore

Magmatic pyrochlore occurs in the calciocarbonatite groundmass (Figure 4a,b), calciocarbonatite xenoliths (Figure 5a) and apatite-magnetite phoscorite xenoliths (Figure 4b). It has a narrow range of composition similar to that of pyrochlore from the carbonatite plug and rings dykes [67,68] but it differs from those because the Y site does not contain F (only up to 1 wt %). The B site is fully occupied by Nb (1.6 to 2.0 apfu) with low Ti contents (0.10–0.20 apfu, being up to 0.32 in apatite-magnetite xenoliths) and extremely low Ta, Zr, Fe and Si (Figure 7a,b). The A position is occupied by Na (from 0.66 to 0.97 apfu) and Ca with no or very low vacancies (Figure 8a). Na may be removed and substituted with up to 2 wt % of $Ce_2O_3$ and $ThO_2$ (Figure 8b,c). Pyrochlore I can be named as hydroxycalciopyrochlore according Atencio [89].

#### 6.1.2. Type II Pyrochlore

Type II pyrochlore is related to subsolidus dolomitization processes and presents significant proportions of Th and REE (groundmass, Figure 4b; carbonatite xenoliths, Figure 5a, Mg-rich xenoliths, Figure 5d). According to its composition, two subtypes are identified, which compositions depend on the compositions of the early pyrochlore replaced and the composition of the hydrothermal fluids. It corresponds to hydroxycalciopyrochlore [89].

- Type IIa—at the A site, Na contents are very low, compensated partly by $ThO_2$ and $Ce_2O_3$ (up to 6.73 and 3.37 wt % respectively). The B site records higher Ti contents than pyrochlore I (up to 0.35 apfu, Figure 7a).
- Type IIb—replaces skeletal crystals of pyrochlore I, apatite and calcite and is intergrown with zirconolite. The A site shows LREE enrichments, especially $Ce_2O_3$ and $Nd_2O_3$ (9.49 and 3.67 wt % respectively, Figure 8b,c). $ThO_2$ is higher than in IIa subtype but lower than the REE sum. Ti content may reach up to 0.48 apfu at the B position.

#### 6.1.3. Type III Pyrochlore

Pyrochlore III overgrows Types I and II, mostly in dolomitized areas (Figure 4b) but appears scarcely in ICML bodies, whereas in the central carbonatite plug and concentric dykes it is abundant [67,68]. Pyrochlore III shows the A site fully occupied by Ca (approximately 1 apfu). High vacancies up to 1 apfu as well as $ThO_2$ and $Ce_2O_3$ (up to 2 wt %) balance charge deficiency. B and Y positions do not present any significant change; therefore, it can be classified as hydroxycalciopyrochlore [89].

#### 6.1.4. Type IV Pyrochlore

The fourth generation of pyrochlore occurs either as individual crystals newly formed during ankeritization (Figure 4c) or as a replacement of primary pyrochlores (Figure 4e). It is very heterogeneous but in general it is characterized by Ta (Figure 7a), Ce, Th and U (Figure 8b,e,f) enrichments when compared with the former pyrochlore generations. At the B site, Nb contents are lower than in the early generations; Ta and Ti cations may reach up to 0.35 and 0.56 apfu respectively. Locally, Si and Zr enrichments may be significant. Significant $UO_2$ content has been recorded in the A site from 1.46 to 22.58 wt %. $ThO_2$ is also remarkable, reaching up to 20.23 wt % where ankeritization is stronger. Vacancies are generally greater than 1 apfu to accommodate the resulting charge deficit. The Y site does not contain F. According to its composition, type IV pyrochlore corresponds to a hydroxykenopyrochlore [89].

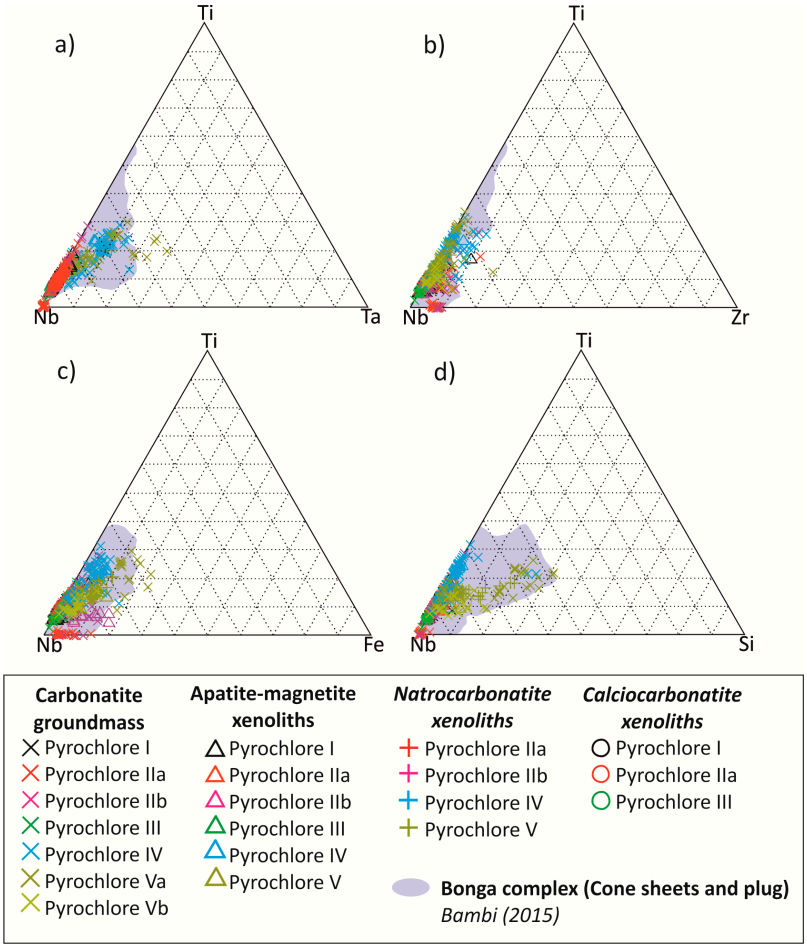


**Figure 7.** Pyrochlore composition subdivided by host unit. Ternary diagrams from (**a**) to (**d**) represent the B site cations. Our results are compared to data from central calciocarbonatite plug, ferrocarbonatite, concentric dykes of calciocarbonatite and carbonatite breccia reported by Bambi [68].

#### 6.1.5. Type V Pyrochlore

Type V pyrochlore is identified in association with ankerite and quartz in late stages of carbonatite formation (Figure 4d). It is characterized by elevated Si and Sr (Figures 7d and 8d) but heterogeneous composition. Two subtypes are distinguished depending on the earlier generation replaced. It is classified as hydroxykenopyrochlore according to Atencio [89].

- Type Va occurs as replacement of type II pyrochlore. The A site contains higher $ThO_2$, $Ce_2O_3$ and Sr contents, up to 0.56 apfu. Significant Si (up to 0.17 apfu) is recorded at the B site when this pyrochlore occurs in areas with extensive hydrothermal quartz replacement.
- Type Vb overgrows type IV pyrochlore, therefore, it displays high $UO_2$ and $ThO_2$ (up to 20.15 wt % and 8.60 wt % respectively) (Figure 8e,f). Sr can reach up to 0.69 apfu but locally may be lower than Ca. Charge balance is compensated by vacancies above 1 apfu. Significant Ti and Ta (up to 0.43 and 0.38 apfu, respectively) and Si contents are determined at B site.

### *6.2. Perovskite*

Perovskite is an accessory mineral identified in the alnöite spherical bodies, calciocarbonatite xenoliths and aillikite groundmass. Magmatic crystals and three secondary types are identified on the basis of distinct compositional and textural characteristics.

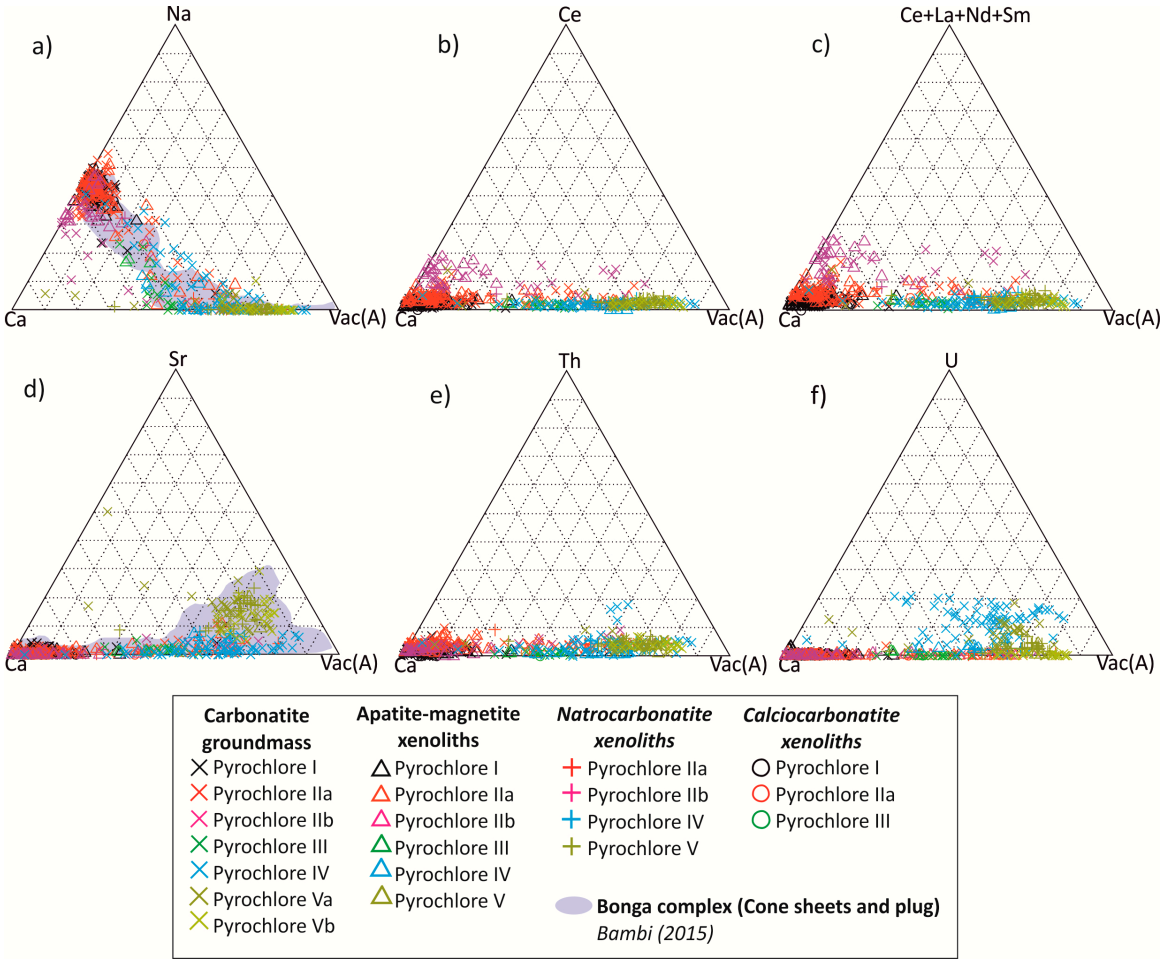


**Figure 8.** Pyrochlore composition subdivided by textural type and host unit. Ternary diagrams from (**a**) to (**f**) represent the A site cations. Our results are compared to pyrochlore data from central calciocarbonatite plug, ferrocarbonatite, concentric dykes of calciocarbonatite and carbonatite breccia reported by Bambi [68].

### 6.2.1. Perovskite Type I

The most common perovskite has compositions near the $CaTiO_3$ end member (Figure 9). Nb, Na, LREE and Fe contents have similarities with the magmatic occurrences described in kimberlite rocks [83,90]. Contents of $Nb_2O_5$ and $Na_2O$ are low, reaching up to 1.90 and 0.5 wt % respectively. Nevertheless, LREE contents range from 1.07 to 2.87 wt % and up to 3.43 wt %. $Ce_2O_3$ is the major REE oxide present. In addition, early perovskite intergrown with magnetite in calciocarbonatite xenoliths has a similar composition but LREE are below 1.88 wt %.

### 6.2.2. Perovskite Types II, III and IV

Type II forms fine rims overgrowing early type I perovskite. High $Nb_2O_5$ contents can range from 2.16 to 7.34 wt %. $Na_2O$ total LREE do not exceed 1.30% and 4.20 wt % respectively. Type II records the highest $ThO_2$ contents, up to 1.38 wt %. Type III perovskite occurs in calciocarbonatite xenoliths replacing types I and II and magnetite. It presents an important lueshite ($NaNbO_3$) end member contribution, having high $Nb_2O_5$ and $Na_2O$ (8.21–28.90 wt % and 0.99–6.34 wt % respectively). Finally, type IV perovskite is found in some cumulates of magnetite-apatite-calcite in the alnöite groundmass. Although its composition is near $CaTiO_3$, it may contain the highest LREE contents (up to 5.79 wt %, Figure 9). $Nb_2O_5$ is also high but $Na_2O$ is not significant.

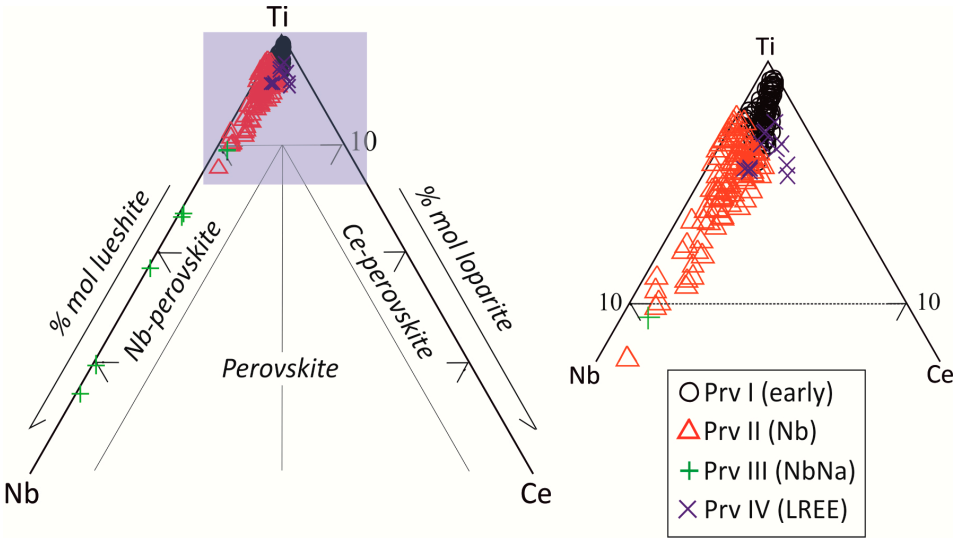


**Figure 9.** Composition of perovskite in the ternary diagram Nb–Ti–Ce [90]. All generations correspond to perovskite s.s. although type III may enter in the Nb perovskite field. The blue field highlights perovskite near to Ti-rich end member.

### *6.3. Baddeleyite*

In magnetite-apatite phoscorites, baddeleyite is replaced by zirconolite and zircon; their compositions approach ideal $ZrO_2$, in spite of remarkable $HfO_2$ and $Nb_2O_5$ contents (1.14 and 1.91 wt %, respectively).

Baddeleyite in the carbonatite groundmass is overgrown by zircon and displays up to 1.35 wt % HfO2, this being the highest proportions recorded in the Bonga complex.

The highest $Nb_2O_5$ contents (up to 7.17 wt %) in baddeleyite crystals have been found in baddeleyite-zirconolite intergrowths in natrocarbonatite xenoliths but also in baddeleyite remnants in pyrochlore crystals (up to 5.44 wt %). Baddeleyite remnants in zirconolite contain significant $Ta_2O_5$, up to 0.73 wt %, being the highest proportions recorded in baddeleyite in the Bonga carbonatite.

### *6.4. Zircon*

Zircon presents homogenous composition near to the $ZrSiO_4$ end member in magnetite-apatite, in natrocarbonatite xenoliths, as well as in the carbonatite groundmass. The $HfO_2$ contents are not very significant and the highest (up to 1.01 wt %) have been recorded in zircon xenocrystals from the carbonatite groundmass. $Nb_2O_5$ may reach 1.97 wt % in zircon from the magnetite-apatite phoscorites.

### *6.5. Zirconolite*

The composition of "zirconolite" minerals from Bonga could fit well in the structural formula of zirkelite. However, the fine grain size of the crystals and their complex intergrowths with other minerals did not allow to extract XRD information. Therefore, following the normative use of mineral nomenclature accepted by the IMA [91], we apply the term zirconolite sensu lato.

Zirconolite has variable $Nb_2O_5$ contents, lower in crystals from the carbonatite groundmass (9.71 to 23.16 wt %) but higher at pyrochlore-zirconolite replacements in apatite-magnetite xenoliths (up to 35.59 wt %). $TiO_2$ and $Nb_2O_5$ correlate negatively, therefore, higher $TiO_2$ proportions are recorded in apatite-magnetite xenoliths. Bonga zirconolite contains notable $Ta_2O_5$ enrichments (0.97 to 3.11 wt %), especially in crystals from the calciocarbonatite groundmass; these contents are similar to those found in zirconolite from Sebl'yavr carbonatite [92]. $ThO_2$ may be up to 6.87wt % in the zirconolite from the groundmass whereas $UO_2$ proportions are generally negligible, well below the limits of acceptance for these elements in the zirconolite structure [93,94]

### *6.6. Nb-Rich Rutile ("Ilmenorutile")*

Ilmenorutile in the carbonatite is associated with dolomite-ankerite and quartz and formed during the hydrothermal stages, usually containing minor amounts of $Nb_2O_5$ (up to 3.24 and 2.36 wt % respectively). However, the Bonga IMCL bodies do not present noticeable Nb enrichments in rutile when compared with the composition of rutile from other carbonatite complexes. In fact, ilmenorutile from the Tchivira carbonatite (10 km SW to Bonga) or Kandaguba (Kola Peninsula) can reach up to 18.86 wt % of $Nb_2O_5$ [25,66].

### *6.7. Phlogopite*

Phlogopite crystals in the phlogopite-apatite-augite xenoliths may presents rare Nb enrichments. Phlogopite-annite solid solution with eastonite and tetraferriphlogopite end member contributions show two types of irregular zoning patterns; the first type shows high $Nb_2O_5$ proportions, up to 2.24 wt % at crystal cores and surrounded by rims of high $Fe_2O_3$ owing to a tetraferriphlogopite component. A second type of phlogopite has Nb rims (up to 1.88 wt % of $Nb_2O_5$) overgrowing $Fe_2O_3$ enriched cores.

## 7. Discussion

### *7.1. Distribution of Minerals with HFSE Elements*

Diverse HFSE-bearing minerals occur in the rock units of the Bonga complex, allowing reconstructions of the evolution of the complex. A synthesis of the distribution of Nb–Ta–Zr–Th–U minerals can be found in Table 1. This table shows the distribution of very early pyrochlore (named here as pyrochlore 0) found in the central units of the Bonga complex and some of the cone sheets [67,68,76].

Early pyrochlore generations (0-II) are the typical primary magmatic mineral in the carbonatitic units of the Bonga intrusion and have the highest tenors of most of the HFSE elements (including Nb, Ta, Ti, U and Th). Zr and Hf can be accommodated also in the primary pyrochlore, although they can also be accommodated rarely in primary baddeleyite. Pyrochlore is rare in the central plug, in part of the cone sheets and in the carbonatitic xenoliths found in the magmatic breccias. However, it is more common in magnetite-phlogopite-apatite-rich carbonatite cone sheets, as it is in the carbonatite groundmass of the magmatic breccias; the highest proportions are achieved in the magnetite-apatite phoscorites. However, it is practically absent in the lamprophyres or in the natrocarbonatites. Secondary pyrochlore generations are found in many of these lithological units where they have been altered (Table 1). Similar late occurrences of pyrochlore are found in many carbonatites such as Tchivira in Angola [67,68,75] or Kovdor in Kola, Russia [95].

Contrastingly, perovskite is the dominant carrier of Nb and Ta in the diverse types of lamprophyres; local occurrences of pyrochlore in the rims of the aillikite spheroids in carbonatite groundmass can be attributed to local contamination by the groundmass. Nb and Ta are accumulated in the last perovskite rims, indicating its late removal from the lamprophyric magma. Zr (and part of Nb and Ta) are also concentrated in these rocks, in minerals of the zirconolite group. These paragenetic differences can be related to a higher Ti activity in the lamprophyres.

Zircon, zirconolite and baddeleyite are absent in most of the rocks of the Bonga complex and is only present in the ICML domains and this fact must be taken into consideration when interpreting the occurrences of this mineral. Baddeleyite is a primary mineral in carbonatites and particularly in phoscorites, as observed in Kovdor in Kola, Russia [33]. Probably there are different generations of minerals of the zirconolite group. Primary zirconolite is found in early pulses of the crystallization of the carbonatite groundmass; magmatic zirconolite has also been described in Kola [33]. However, when present in the ICML domains, zirconolite tends to replace Nb- or Zr- bearing minerals, such as pyrochlore and zircon. A similar trend has been observed in the Kovdor carbonatite [96,97]. Some of these replacement processes are associated with ankeritization; therefore, this zirconolite could be produced during the hydrothermal stages, as suggested in Table 1. Moreover, the existence of

intimate mixtures of different rocks may favour the development of a complex paragenesis during the simultaneous hydrothermal alteration of all these rocks. As indicated, the existence of different generations of pyrochlore demonstrates the mobilisation of Nb (and Ta) in the subsolidus stages of the carbonatite evolution and different subsolidus processes also remove Ti in the lamprophyres. Therefore, the simultaneous removal of Nb, Zr and Ti in the different units of the ICML mixtures during late hydrothermal processes may explain the widespread precipitation of late zirconolite and ilmenite. Transport of these HFSE is very effective in hydrothermal fluids associated with alkaline magmatism [98–100] and fenitization provides evidence of the large-scale movement of alkaline fluids associated with carbonatite intrusions. Moreover, circulation of alkaline fluids in the lamprophyres is indicated by pervasive hydrothermal processes resulting in the widespread occurrence of aspidolite replacing the previous silicates. The transport of these elements could be effective over limited distances because zirconolite is restricted to ICML domains. Complex zoning in zirconolite can be easily explained by lack of equilibria during the crystallization from the solutions. Minerals of the zirconolite group and baddeleyite seem to be largely unstable in the presence of silica in solution during the late stages of crystallization, which could explain their replacement by zircon.

**Table 1.** Distribution of minerals with HFSE in the rocks of the Bonga complex.

| Unit | | Primary HFSE Minerals | Subsolidus HFSE Minerals | |
|---|---|---|---|---|
| | | | Dolomitization/ Ankeritization | Silicification |
| Carbonatite Plug | carbonatite groundmass | Pyrochlore 0<br>Pyrochlore II | Pyrochlore III<br>Pyrochlore IV | Pyrochlore V |
| Carbonatite Cone Sheets | carbonatite groundmass | Pyrochlore 0<br>Pyrochlore II | Pyrochlore III<br>Pyrochlore IV | Pyrochlore V |
| ICML Domains with Carbonatite Groundmass | carbonatite groundmass | Pyrochlore I<br>Pyrochlore II<br>Baddeleyite | Pyrochlore III<br>Pyrochlore IV<br>Zirconolite<br>Thorutite<br>Uranothorianite | Pyrochlore V<br>Zircon Ilmenorutile |
| | aillikite spheroids | Perovskite I<br>Perovskite II<br>Pyrochlore I | | |
| | apatite-magnetite phoscorite xenoliths | Pyrochlore I<br>Pyrochlore II (Nb) | Pyrochlore III<br>Pyrochlore IV<br>Zirconolite | Pyrochlore V<br>Zircon Ilmenorutile |
| | phoscorite xenoliths | | Zirconolite | Zircon<br>Lucasite-(Ce)<br>Kassite |
| | magnesian xenoliths | Pyrochlore I<br>Pyrochlore II (Nb) | Pyrochlore III<br>Pyrochlore IV | Aeschynite<br>Vigezzite<br>Pyrochlore V |
| | natrocarbonatite xenoliths | Calzirtite (?) | Zirconolite<br>Ilmenorutile | Zircon Pyrochlore V |
| ICML Domains with Aillikite Groundmass | aillikite groundmass | Perovskite I<br>Perovskite II (Nb) | Zirconolite | |
| | alnoite spheroids | Perovskite I<br>Perovskite II (Nb) | | Perovskite III<br>Perovskite IV |
| | phlogopite-apatite xenoliths | Nb-phlogopite<br>Nb-augite Ilmenite | | Ilmenorutile |
| | calciocarbonatite xenoliths | Calzirtite Perovskite | Zirconolite<br>Perovskite III | |
| | turjaite xenoliths | Perovskite | | |

Finally, Nb-bearing phlogopite have been found in glimmeritic xenoliths. The discussion of Nb in these minerals is beyond the scope of this study and will be discussed elsewhere.

### *7.2. Compositional and Textural Variation of Primary Magmatic Pyrochlore*

As observed, pyrochlore I crystals show almost constant compositions in the calciocarbonatite xenoliths, magnetite-apatite rocks and calciocarbonatite groundmass of the ICML bodies, although some differences occur. Generally, Na and Ca are the major cations at the A site, with lesser Th, U, Ce, Sr and vacancies. However, U content is higher in magnetite–apatite rocks where it correlates positively with Ta and Ti in the B site. In addition, carbonatite groundmass presents slightly more evolved composition as suggested by higher contents of Si and Zr in pyrochlore I.

To illustrate the behaviour of F in early pyrochlore, F is plotted against HFSE, REE and LILE and compared with the rest of the Bonga units and with those from other Angolan complexes—Tchivira, Bonga and Catanda, representative of plutonic, hypabyssal and volcanic carbonatites, respectively (Figure 10). Pyrochlore I of the ICML bodies of Bonga shows extremely low F but with similar trends as in the other Angolan occurrences, including pyrochlore 0 from the plug and dykes. F is even lower than in the extrusive Catanda carbonatites, where the low F has been related to exsolution of F-bearing fluid from the carbonatite magma during explosive processes [67,68]. F depletion in the ICML carbonatite groundmass is another argument to indicate that these units were formed late during the carbonatite processes, after the crystallisation of early F-rich magmas. The occurrence of pyrochlore I both in the breccias and in the carbonatite xenoliths with more evolved compositions than those of pyrochlore 0 means that type I pyrochlore also crystallized in magmatic conditions but in a more advanced stage than type I.

Finally, the other important change in primary pyrochlore during the crystallization sequences is the change in the textural patterns. Pyrochlore crystals from the plug or the concentric dykes, as well as those found in the carbonatite xenoliths, tend to have an euhedral shape and the grain size can be up to 2 mm in diameter. Even though in some cases it may show intergrowths with apatite and magnetite, it is normally free from other mineral inclusions. These textures are favourable for the extraction of these crystals during the industrial beneficiation of the ores. However, the textures in the breccia groundmass, produced in a disequilibrium context, tend to be more complex; skeletal intergrowths with other minerals add a problem for the beneficiation, reduced grain size and the scarcity of the mineral is also a problem. Some of these issues could also be extended to the Nb-bearing minerals from the lamprophyric rocks.

The breccias contain fragments of phoscoritic rocks, thus indicating that at least part of the richest mineralization could had been dispersed. Therefore, the existence of explosive processes in the carbonatites can reduce the interest of a given deposit but potentially lead to an unfragmented exploration target.

### *7.3. Pyrochlore as Indicator of the Dynamics of the Carbonatite Crystallization*

Apatite, pyrochlore, magnetite, phlogopite and amphibole are characteristic minerals of carbonatites [7]. Indeed, they appear in most of the studied Angolan carbonatites such as Tchivira [66,68], Bailundo [101], Virulundo [71], Bonga [67,68,70,76,88] and Monte Verde [69,70] but pyrochlore is irregularly distributed and has different compositions. In the Angolan carbonatite complexes, the highest pyrochlore concentrations usually occur in the calciocarbonatite concentric dykes (pyrochlore 0 with high F and Na) and magnetite-apatite phoscoritic rocks (pyrochlore I with low F and high Na), as well as in the calciocarbonatite groundmass of the external IMCL bodies of Bonga (pyrochlore I with low F and high Na), as observed in this work, instead of being enriched in the central calciocarbonatite plugs.

Pyrochlore generally reaches the highest modal proportions inside apatite-magnetite phoscorite bodies, which can be interpreted as cumulates. Large phoscoritic bodies with identical strong pyrochlore enrichments also appear in the Bailundo carbonatite [101]. In addition, as described for the Brazilian carbonatite complexes belonging to the Paraná-Angola-Namibia carbonatite province,

such as Salitre [102], Morro do Padre at the Catalão carbonatite [103] and Catalão I complex [104], Nb accumulates preferentially in phoscorites and carbonatites enriched in apatite-magnetite. On the other hand, and as it was already pointed out in previous works [88], there is a good positive correlation between the pyrochlore grade and the increasing proportion of magnetite and apatite in the banded carbonatites of the central plug and in the concentric dykes around Bonga. Hence, pyrochlore is lacking in carbonatite dykes and bands without magnetite and apatite, whereas intermediate concentrations of pyrochlore crystals are found in some of the concentric dykes with accessory proportions of these minerals.

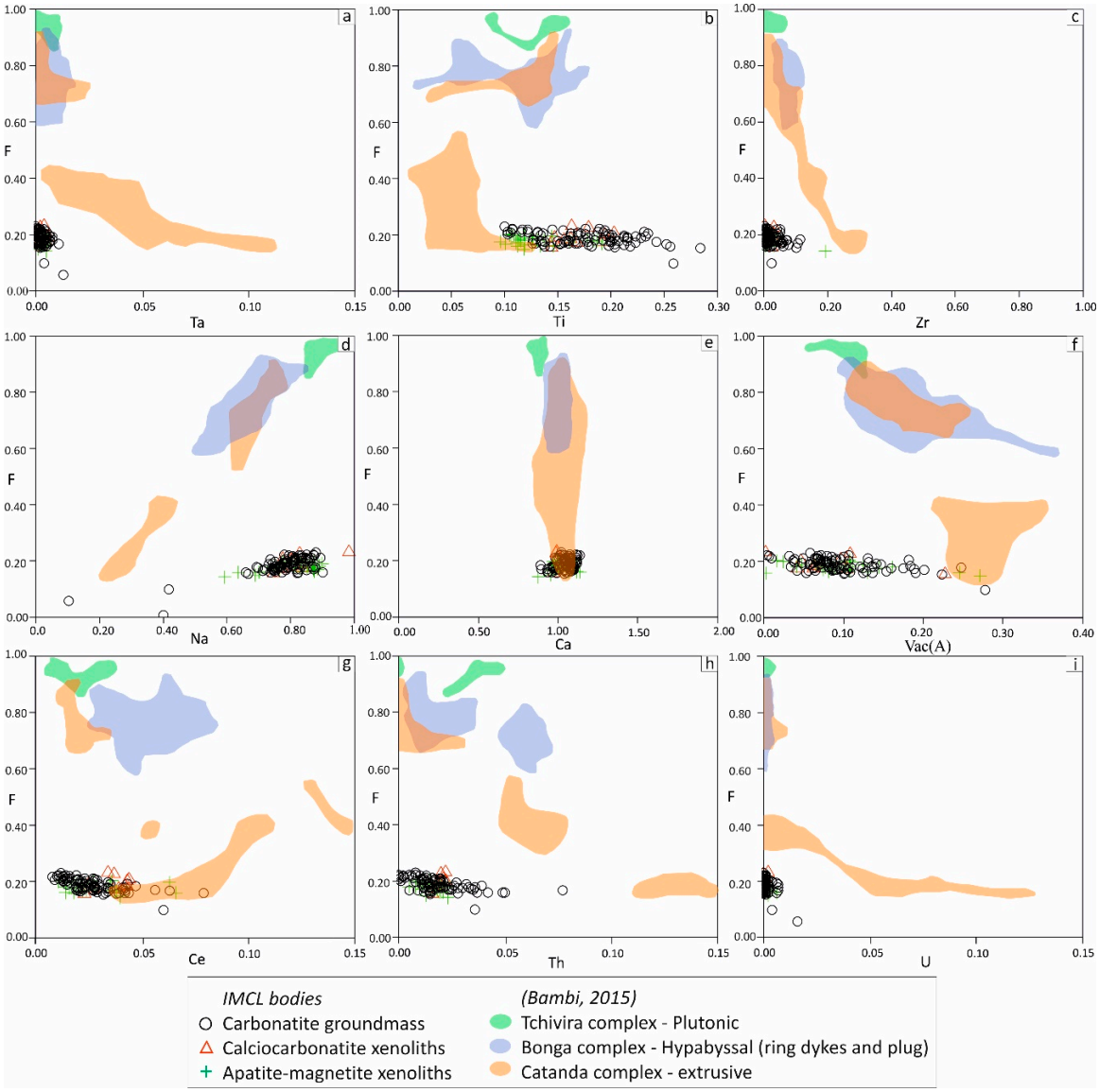


**Figure 10.** HFSE, LILE and REE vs. F in primary magmatic pyrochlore at the ICML bodies of carbonatite groundmass. (**a**) to (**c**) binary diagrams correspond to B-site variations whereas (**d**) to (**i**) represent A-site changes. Our results are compared with primary pyrochlore data from the plutonic carbonatites of Tchivira (green area), primary pyrochlore 0 from the central units of Bonga (blue region) and primary pyrochlore from the volcanic complex of Catanda (orange) reported by Bambi [68].

The main mechanism of pyrochlore accumulation could be explained by crystal fractionation processes, because apatite, magnetite and pyrochlore correspond to the higher density and earlier crystallization phases in these magmas [32]. The Bonga carbonatite bodies normally present banding textures, which may suggest magmatic fluxes [68]. Therefore, the fractional crystallization of liquidus

phases in a low viscous magma affected by convection processes would concentrate dense crystals towards outer and colder margins of the magma chamber. However, pyrochlore 0 and I did not crystallize in a single pulse, because they differ, mainly in the proportions of F, thus indicating very different F activities in the magma from which they precipitated. Hence, an accumulation of F should be produced before the crystallization of the pyrochlore type I and therefore, before the crystallization of the magnetite-apatite-pyrochlore phoscorites.

Successive pulses of intrusion and eruption could help to mobilize part of these magmas, with variable crystal content, towards the cone sheets, thus producing the enrichment of pyrochlore, apatite and magnetite (type 0 pyrochlore, typical of the centre of the plug and the concentric dykes) in some of these dykes. Hence, the extraction of magma from the outer part of the intrusion could release a higher proportion of cumulates.

On the other hand, the existence of aillikite and alnöite spheroids can be interpreted as evidences of magma mingling. Hence, successive intrusion of immiscible lamprophyre magmas and its partial crystallization and degassing caused when entering into contact with a cooler magma, could have favoured the overpressure of the magma chamber leading to its rupture [105–107]. This cracking of the host rock would have favoured degassing and displacement of carbonatite magmas through the margins of the magma chamber, which could be enriched in pyrochlore and may also form cone sheets intruding from the magma chamber towards the surface, enriched in dense phases.

Pyrochlore II can be present in some weakly altered occurrences and could be, at least in part, primary. It tends to overgrow pyrochlore I but it can also form discrete crystals. It is characterized by decreasing Na proportions, down to undetected. This trend, which is common in most of the studied carbonatites in Angola and worldwide, could be related to a progressive reduction of the Na activity in the carbonatite magma during the late stages of crystallization. Furthermore, crystallization from an evolved carbonatitic magma could also explain their higher contents in incompatible elements such as HFSE (as Th and U) and REE than type 0 and I pyrochlores.

The rest of the pyrochlore generations are associated with quartz or secondary carbonates and therefore they must form part of the subsolidus history of the carbonatite.

To sum up, the following stages of the crystallization of the complex are inferred by the pyrochlore mineral chemistry (Figure 11):

- Carbonatite magma ascended and formed a magma chamber. Radial dykes and cone-sheet fractures were produced into the country rocks by overpressure, probably as a result of fluid exsolution in the magma chamber. Early intrusive episodes may have produced carbonatite cone sheets dykes without mineralization of apatite, magnetite or pyrochlore. Early carbonatite magma could have had a natrocarbonatite component as suggested by the composition of the early pyrochlore 0 and I compositions (high Na proportion [67,68,76,88]). Liquidus minerals, such as pyrochlore 0, magnetite and apatite, were concentrated in the margins of magma chamber due to convective processes (Figure 11A). Successive intrusive episodes caused the extraction of these marginal magmas, slightly enriched in pyrochlore 0, towards a new set of concentric dykes, which are mineralized. During this, most of F was removed from the magma.
- The progressive crystallization of the F-poor magma account accompanies the growth of pyrochlore I, forming phoscoritic cumulates in the outer zone of the carbonatite plug along with magnetite and apatite. At the same time, fenitization processes of the country rock progressed; therefore, the carbonatite magma became progressively impoverished in Na (Figure 11B) also due to fenitization.
- Continuous magma intrusion created new cone sheet fractures, probably leading to eruptions at surface. Magma from the chamber margins, enriched in pyrochlore type I, apatite and magnetite, filled new fractures. Fenitization of hosting granite progressed (Figure 11B).
- Fractionation of dense minerals (apatite, magnetite and pyrochlore type I) occurred at the margins of the chamber. Simultaneously, aillikite and alnöite magmas intruded into the carbonatite magma chamber and, spheroidal bodies with immiscibility textures form. This mingling may have triggered explosive episodes resulting in the formation of the carbonatite breccias surrounding

the plug (Figure 11B). Pyrochlore type II (without Na in the A position) was probably formed at the end of this stage or early in the next one and reflects the very low Na activity in the magma that could be related to the end the fenitization processes.

- After cooling and crystallization of the magma chamber, pervasive Mg-rich fluids generated dolomitization. Pyrochlore III was formed in this stage and does not contain Na. Then, ankeritization replacement caused the formation of pyrochlore type IV containing high proportions of U, Ta and Th (Figure 11C).
- At late stages, meteoric hot fluids invaded the carbonatite and caused the extensive formation of quartz. Pyrochlore type V with high Si, Sr and the highest LREE, U, Ta and Th proportions crystallized during this episode (Figure 11D). Replacement of primary carbonates and phosphates may have released large amounts of Sr, REE from the primary carbonates, thus producing strontianite and LREE carbonates and phosphates.

Besides, weathering of the carbonatites produced large pyrochlore concentrations in colluvial sediments and lateritic ores at the external margins of the complex. Therefore, lateritic concentrations may be critical to form economic pyrochlore accumulations [4,5,108–111].

### *7.4. REE Distribution*

The Bonga magmatic pyrochlore shows lower REE contents than late hydrothermal pyrochlore (types II, IV and V). Alike, REE minerals may correspond to late hydrothermal products related to secondary dolomite, ankerite, barite and quartz. Quartz dissolved from the host rock, probably during the fenitization processes, formed hydrothermal fluids once the carbonatites crystallized. Therefore, if the REE carbonates and phosphates are intergrown with late quartz, they cannot have crystallized during magmatic conditions and must have formed during deuteric processes.

$\delta^{13}C$ and $\delta^{18}O$ isotopic data of Bonga carbonates (magmatic calcite—$\delta^{13}C$ from −6‰ to −4.5 ‰ and $\delta^{18}O$ from 7.5 to 8.5‰; late calcite, dolomite and ankerite—$\delta^{13}C$ from −8‰ to −3‰ and $\delta^{18}O$ from 5‰ to 10‰ but up to 24‰ [68]) indicate the influence of late fluids of meteoric origin in most secondary carbonate crystallization, which would be responsible for late dolomitization, ankeritization and silicification processes affecting the primary calciocarbonatite [68,112].

The REE mineral may have been derived from breakdown of primary carbonates and phosphates, as in carbonatites these phases are usually enriched in these elements [46,113]. The neoformation of secondary carbonates at lower temperature would not have been able to reassimilate the REE released from the primary carbonate dissolution. Therefore, the higher abundance of secondary carbonates in the outer carbonatite plug, concentric dykes and breccia rather than at the central carbonatite plug can be explained by greater interaction with low-temperature fluids in the marginal units. REE minerals precipitate as REE carbonates or phosphates depending on $CO_3^{2-}$ and $PO_4^{3-}$ activities of the fluid [51,114]. For that reason, synchysite-(Ce) is the main REE mineral at the Bonga complex; however, REE phosphates can be formed as subsolidus products in primary apatite-rich units.

### *7.5. Role of Magma Mingling on the Concentration of Critical Elements in Carbonatites*

Entry of immiscible magmas in magma chambers can trigger explosive eruptions [115]. These explosive processes, therefore, can be associated with the overpressure leading to the emplacement of the mineralized cone sheets at Bonga, probably by expulsion of fractionated phoscoritic magmas enriched in pyrochlore from the magma chamber. Removal of supercritic fluids during these explosive processes could also be an effective mode of releasing the complexing ligands for the critical metals, thus forcing them to precipitate in large scale during these stages. Hence, the evidence of magma mingling in Bonga can explain the high tenors in HFSE in the cone sheets, which contrast with the low tenors found in the rest of the carbonatite.

The entrance of lamprophyric magmas did not produce a significant input of critical elements in the magma chamber and both types of magmas crystallized separately.

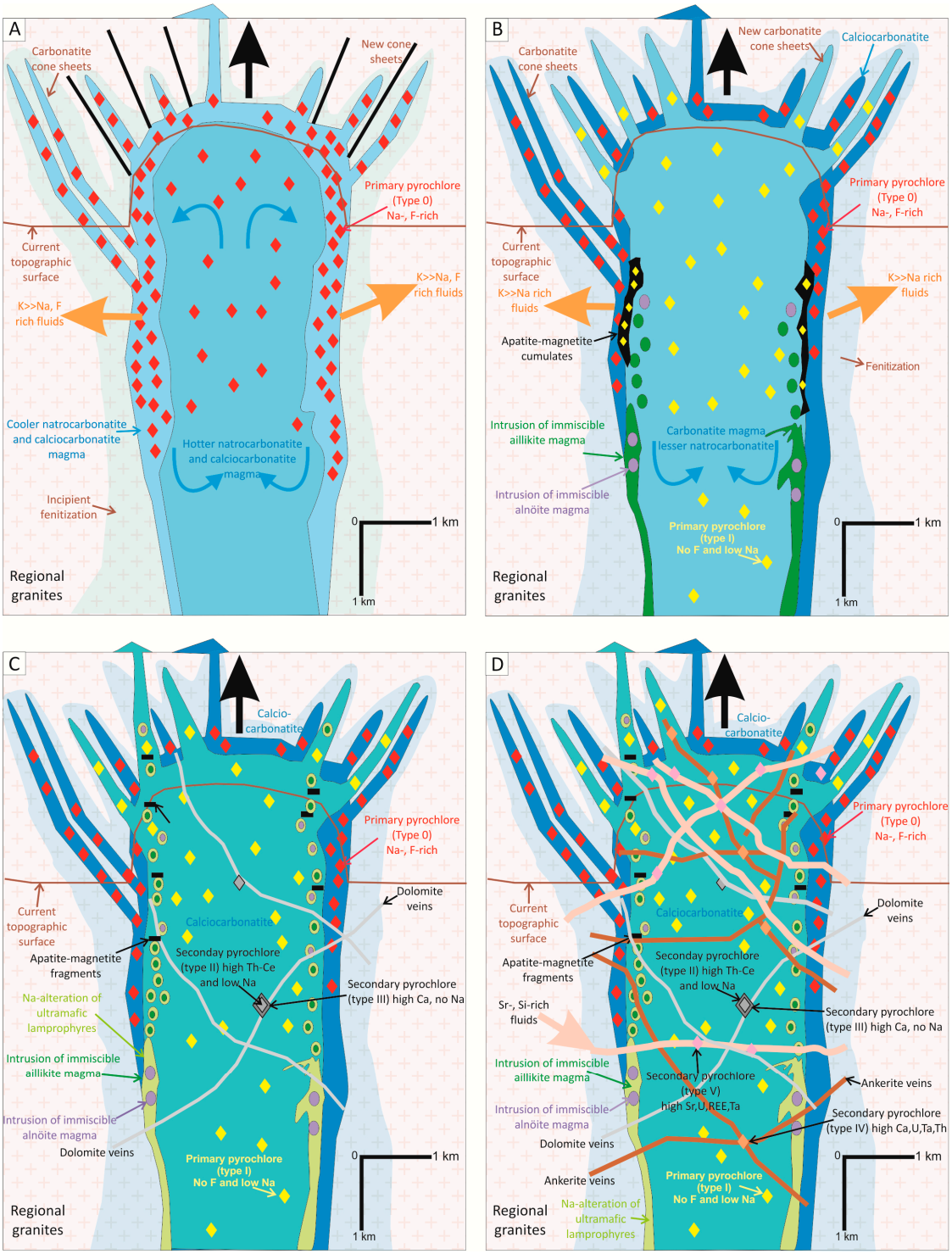


**Figure 11.** Magmatic and hydrothermal evolution of the Bonga carbonatite. (**A**) Early intrusion of carbonatite magma, formation of radial fractures and cone-sheets in the host rock, crystallization of pyrochlore 0 with high Na and F; fenitization starts; (**B**) formation of apatite-magnetite cumulates and intrusion of alnöite and aillikite magma at margins coupled with strong degasification; fenitization progress, loss of Na activity in the magma with crystallization of pyrochlore I without F; late crystallization stages start produce pyrochlore II without Na owing to alkali release during fenitization; (**C**) Once the calciocarbonatite plug crystallizes, fenitization process stopes and dolomite alteration affects the whole complex as pyrochlore II and III record; (**D**) Late stages. Ankerite as well as Si, Sr-rich hydrothermal fluids replace the ensemble. Late pyrochlores IV, V and VI are enriched in HFSE.

## 8. Concluding Remarks

The good correlation between magnetite and pyrochlore contents, with the highest proportion of pyrochlore in phoscorites, suggest that the best places to find large pyrochlore deposits are the carbonatite concentric dykes and the phoscorites. The occurrence of increased apatite contents in these domains add another possible resource of a critical raw material in the same units. The most favourable sites seem to be the top and the margins of the intrusions, as well as some of cone sheets.

Conversely, the main plug and the early concentric dykes (or cone-sheets) have scarce pyrochlore or may be considered as barren. Therefore, the use of magnetometric methods of exploration can be very helpful in localizing large reserves of pyrochlore in Bonga and many similar carbonatites in Angola and worldwide. However, caution must be taken when there is evidence of magnetite-bearing lamprophyres. In this sense, the existence of carbonatite breccia can directly reveal the existence of these intrusions, by localizing the corresponding xenoliths or mingled units. The existence of these bodies at depth can probably be inferred indirectly, because magma mingling may favour explosive processes, which can have a negative metallogenetic role because they disperse the mineralization and produce complex textures that can make difficult the industrial concentration of ores.

The lamprophyric units seem to lack economic mineralization of critical elements but they may carry out a determinant influence in the explosive processes leading to redistribute the ores and producing textures unfavourable for ore formation.

The highest contents in other critical metals, particularly Ta, are found in association with the latest hydrothermal processes and these have generally affected the carbonatite irregularly. However, these processes are more intense at the margins and at the top of the intrusions and, therefore, these units can also be targeted for critical elements. Finally, the REE are concentrated in the strongest ankeritized and silicified domains.

**Supplementary Materials:** The mineral chemistry analyses of pyrochlore, baddeleyite, ilmenorutile, zirconolite and perovskite are available online at http://www.mdpi.com/2075-163X/9/10/601/s1.

**Author Contributions:** Conceptualization, S.A.-C. and J.-C.M.; methodology, S.A.-C., J.-C.M., A.C., A.B.; investigation, S.A.-C., J.-C.M., A.B., A.O.G., E.A.M., A.B.N., J.M.; writing—original draft preparation, S.A.-C.; writing—review and editing, J.-C.M., J.M.M., A.C.; visualization, S.A.-C., J.-C.M., J.M.M.: funding acquisition, J.-C.M.

**Funding:** This research was funded by Ministerio de Ciencia e Innovación (Spain), grants number CGL2006-12973 and CGL2009-13758, the 2017 SGR 0707 of the AGAUR-Generalitat de Catalunya and a Ph.D. grant to S. Amores-Casals sponsored by the Generalitat de Catalunya; the Hugh. E. McKinstry fund grant from the Society of Economic Geologist to carry out field work in Angola. Logistic assistance for the field trips was provided by the Departmento de Geologia da Universidade Agostinho Neto (Luanda, Angola). The Ph.D. studies of A. Bambi in Barcelona were supported by an AECI grant. A. Costanzo acknowledges financial support provided by the SYNTHESIS (Project GB-TAF-3835).

**Acknowledgments:** Xavier Llovet helped in the preparation of EPMA analyses at the Serveis Científico-Tècnics, Universitat de Barcelona. The reviewing of two anonymous referees helped to improve the manuscript.

**Conflicts of Interest:** The authors declare no conflict of interest. The funders had no role in the design of the study; in the collection, analyses, or interpretation of data; in the writing of the manuscript, or in the decision to publish the results.

## References

1. Woolley, A.R.; Kempe, D.R.C. Carbonatites: Nomenclature, average chemical compositions and element distributions. In *Carbonatite: Genesis and Evolution*; Bell, K., Ed.; Unwin Hyman: London, UK, 1989; pp. 1–14.
2. Mitchell, R.H. Carbonatites and carbonatites and carbonatites. *Can. Mineral.* **2005**, *43*, 2049–2068. [CrossRef]
3. Woolley, A.R. *Alkaline Rocks and Carbonatites of the World. Part 3. Africa*; Geological Society of London: London, UK, 2001; p. 372.
4. Mariano, A.N. Nature of economic mineralization in carbonatites and related rocks. In *Carbonatite: Genesis and Evolution*; Bell, K., Ed.; Unwin Hyman: London, UK, 1989; pp. 149–176.
5. Mariano, A.N. Economic Geology of Rare Earth Elements. *Rev. Mineral.* **1989**, *21*, 309–337.

6. Knudsen, C. Pyrochlore-group minerals from the Qaqarssuk carbonatite complex. In *Lanthanides, Tantalum and Niobium*; Möller, P., Černý, P., Saupé, F., Eds.; Springer: Berlin/Heidelberg, Germany, 1989; pp. 80–99.
7. Hogarth, D.D. Pyrochlore, apatite and amphibole: distinctive minerals in carbonatite. In *Carbonatite: Genesis and Evolution*; Bell, K., Ed.; Unwin Hyman: London, UK, 1989; pp. 105–148.
8. Verwoerd, W.J.; Viljoen, E.A.; Chevallier, L. Rare metal mineralization at the Salpeterkop carbonatite complex, Western Cape Province, South Africa. *J. Afr. Earth Sci.* **1995**, *21*, 171–186. [CrossRef]
9. Pell, J. Mineral deposits associated with carbonatites and related alkaline igneous rocks. In *Undersaturated Alkaline Rocks: Mineralogy, Petrogenesis and Economic Potential*; Mitchell, R.H., Ed.; Mineralogical Association of Canada: Quebec City, QC, Canada, 1996; pp. 271–310.
10. Palmer, D.A.S.; Williams-Jones, A.E. Genesis of the carbonatite-hosted fluorite deposit at Amba Dongar, India: Evidence from fluid inclusions, stable isotopes and whole rock-mineral geochemistry. *Econ. Geol.* **1996**, *91*, 934–950. [CrossRef]
11. Wall, F.; Mariano, A.N. Rare earth minerals in carbonatites a discussion centered on the Kangankunde Carbonatite, Malawi. In *Rare Earth Minerals: Chemistry, Origin and Ore Deposit*; Jones, A.P., Wall, F., Williams, C.T., Eds.; Chapman & Hall: London, UK, 1996; pp. 193–225.
12. Richardson, D.G.; Birkett, T.C. Carbonatite-associated Deposits. In *Geology of Canadian Mineral Deposit Types*; Eckstrand, O.R., Sinclair, W.D., Thorpe, R.I., Eds.; Geological Survey of Canada: Ottawa, ON, Canada, 1996; pp. 541–558.
13. Wall, F.; Williams, C.T.; Woolley, A.R. Pyrochlore from weathered carbonatite at Lueshe, Zaire. *Mineral. Mag.* **1996**, *60*, 731–750. [CrossRef]
14. Wall, F.; Zaitsev, A.N.; Le Bas, M.J. REE-Sr-Ba minerals from the Khibina carbonatites, Kola peninsula, Russia: Their mineralogy, paragenesis and evolution. *Mineral. Mag.* **1998**, *62*, 225–250.
15. Wall, F.; Williams, C.T.; Woolley, A.R. Pyrochlore in niobium ore deposits. Mineral deposits: Processes to processing. In Proceedings of the Fifth Biennial SGA Meeting and the Tenth Quadrennial IAGOD Symposium, London, UK, 22–25 August 1999; pp. 687–690.
16. Wall, F.; Sitnikova, M.A.; Zaitsev, A.N.; Chakhmouradian, A.R.; Subbotin, V.V. Evolution of chemical composition of rock-forming carbonates in Sallanlatvi Carbonatites, Kola Peninsula, Russia. *J. Afr. Earth Sci.* **2001**, *32*, A34.
17. Wall, F.; Broom-Fendley, S.; do Cabo, V.; Dowman, E. Rare earth deposits associated with carbonatite complexes—Where are the heavy rare earths? *Can. Mineral.* **2008**, *46*, 861. [CrossRef]
18. Wall, F.; Niku-Paavola, V.N.; Storey, C.; Müller, A.; Jeffries, T. Xenotime-(Y) from carbonatite dykes at Lofdal, Namibia: Unusually low LREE:HREE ratio in carbonatite and the first dating of xenotime overgrowths on zircon. *Can. Mineral.* **2008**, *46*, 861–877. [CrossRef]
19. Chakhmouradian, A.R. On the development of niobium and rare-earth minerals in monticellite-calcite carbonatite of the Oka Complex, Quebec. *Can. Mineral.* **1996**, *34*, 479–484.
20. Chakhmouradian, A.R.; Mitchell, R.H. Lueshite, pyrochlore and monazite-(Ce) from apatite-dolomite carbonatite, Lesnaya Varaka complex, Kola peninsula, Russia. *Mineral. Mag.* **1998**, *62*, 769–782. [CrossRef]
21. Bulack, A.G.; Le Bas, M.J.; Wall, F.; Zaitsev, A.N. Ancylite-bearing carbonatites of the Sebl'yavr massif, Kola Peninsula, Russia. *Neues Jahrb. Mineral. Monatsh.* **1998**, 171–192.
22. Bulakh, A.G.; Nesterov, A.R.; Zaitsev, A.N.; Pilipiuk, A.N.; Wall, F.; Kirillov, A.S. Sulfur containing monazite-(Ce) from late stage mineral assemblages at the Kandaguba and Vuoriyarvi carbonatite complexes, Kola peninsula, Russia. *Neues Jahrb. Mineral. Monatsh.* **2000**, *5*, 217–233.
23. Chakhmouradian, A.R.; Reguir, E.P.; Zaitsev, A.N. Calcite and dolomite in intrusive carbonatite. I. Textural variations. *Miner. Petrol.* **2015**, *2–3*, 333–360. [CrossRef]
24. Hogarth, D.D.; Williams, C.T.; Jones, P. Primary zoning in pyrochlore group minerals from carbonatites. *Mineral. Mag.* **2000**, *64*, 683–697. [CrossRef]
25. Pilipiuk, A.N.; Ivanikov, V.V.; Bulakh, A.G. Unusual rocks and mineralization in a new carbonatite complex at Kandaguba, Kola Peninsula, Russia. *Lithos* **2001**, *56*, 333–347. [CrossRef]
26. Groves, D.I.; Vielreicher, N.M. The Phalabowra (Palabora) carbonatite-hosted magnetite-copper sulfide deposit, South Africa: an end member of the iron-oxide-copper-gold-rare earth elements deposit group? *Miner. Deposita.* **2001**, *136*, 189–194. [CrossRef]

27. Bühn, B.; Rankin, A.H.; Schneider, J.; Dulski, P. The nature of orthomagmatic, carbonatitic fluids precipitating REE, Sr-rich fluorite: Fluid inclusion evidence from the Okorusu fluorite deposit, Namibia. *Chem. Geol.* **2002**, *186*, 75–98. [CrossRef]
28. Chakhmouradian, A.R.; Mitchell, R.H. New data on pyrochlore- and perovskite group minerals from the Lovozero alkaline complex, Russia. *Eur. J. Mineral.* **2002**, *14*, 821–836. [CrossRef]
29. Krasnova, N.I.; Petrov, T.G.; Balaganskaya, E.G.; Garcia, D.; Wall, F.; Moutte, J.; Zaitsev, A.N. Introduction to phoscorites: Occurrence, composition, nomenclature and petrogenesis. In *Phoscorites and Carbonatites from Mantle to Mine: The Key Example of the Kola Alkaline Province*; Wall, F., Zaitsev, A.N., Eds.; Mineralogical Society of Great Britain and Ireland: London, UK, 2004; pp. 43–72.
30. Zurevinski, S.E.; Mitchell, R.H. Extreme compositional variation of pyrochlore group minerals at the Oka Carbonatite Complex, Québec: evidence of magma mixing? *Can. Mineral.* **2004**, *42*, 1159–1168. [CrossRef]
31. Lee, M.J.; Garcia, D.; Moutte, J.; Wall, F.; Williams, C.T. Carbonatites and phoscorites from the Sokli Complex, Finland. In *Phoscorites and Carbonatites from Mantle to Mine: The Key Example of the Kola Alkaline Province*; Wall, F., Zaitsev, A.N., Eds.; Mineralogical Society of Great Britain and Ireland: London, UK, 2004; pp. 129–158.
32. Lee, M.J.; Lee, J.I.; Garcia, D.; Moutte, J.; Williams, C.T.; Wall, F.; Kim, Y. Pyrochlore chemistry from the Sokli phoscorite-carbonatite complex, Finland: Implications for the genesis of phoscorite and carbonatite association. *Geochem. J.* **2006**, *40*, 1–13. [CrossRef]
33. Chakhmouradian, A.R.; Williams, C.T. Mineralogy of high-field-strength elements (Ti, Nb, Zr, Ta, Hf) in phoscoritic and carbonatitic rocks of the Kola Peninsula, Russia. In *Phoscorites and Carbonatites from Mantle to Mine: The Key Example of the Kola Alkaline Province*; Wall, F., Zaitsev, A.N., Eds.; Mineralogical Society of Great Britain and Ireland: London, UK, 2004; pp. 293–337.
34. Wall, F.; Zaitsev, A.N. Rare earth minerals in Kola carbonatites. In *Phoscorites and Carbonatites from Mantle to Mine: The Key Example of the Kola Alkaline Province*; Wall, F., Zaitsev, A.N., Eds.; Mineralogical Society of Great Britain and Ireland: London, UK, 2004; pp. 43–72.
35. Xu, C.; Kynicky, J.; Chakhmouradian, A.R.; Qi, L.; Song, W. A unique Mo deposit associated with carbonatites in the Qinling orogenic belt, central China. *Lithos* **2010**, *118*, 50–60. [CrossRef]
36. Xu, C.; Wang, L.; Song, W.; Wu, M. Carbonatites in China: A review for genesis and mineralization. *Geosci. Front.* **2010**, *1*, 105–114. [CrossRef]
37. Xu, C.; Taylor, R.N.; Li, W.; Kynicky, J.; Chakhmouradian, A.R.; Song, W. Comparison of fluorite geochemistry from REE deposits in the Panxi region and Bayan Obo, China. *J. Asian Earth Sci.* **2012**, *57*, 76–89. [CrossRef]
38. Doroshkevich, A.G.; Ripp, G.S.; Viladkar, S.G.; Vladykin, N.V. The Arshan REE carbonatites, Southwestern Transbaikalia, Russia: Mineralogy, paragenesis and evolution. *Can. Mineral.* **2008**, *46*, 807–823. [CrossRef]
39. Yang, K.F.; Fan, H.R.; Santosh, M.; Hu, F.F.; Wang, K.Y. Mesoproterozoic carbonatitic magmatism in the Bayan Obo deposit, Inner Mongolia, North China: Constraints for the mechanism of super accumulation of rare earth elements. *Ore Geol. Rev.* **2001**, *40*, 122–131. [CrossRef]
40. Chakhmouradian, A.R.; Wall, F. Rare earth elements: minerals, mines, magnets (and more). *Elements* **2012**, *8*, 333–340. [CrossRef]
41. Chakhmouradian, A.R.; Zaitsev, A.N. Rare earth mineralization in igneous rocks: Sources and processes. *Elements* **2012**, *8*, 347–353. [CrossRef]
42. Zaitsev, A.N.; Chakhmouradian, A.R.; Siidra, O.I.; Spratt, J.; Williams, C.T.; Stanley, C.J.; Petrov, S.V.; Britvin, S.N.; Polyakova, E.A. Fluorine-, yttrium- and lanthanide-rich cerianite from carbonatitic rocks of the Kerimasi volcano and surrounding explosion craters, Gregory Rift, northern Tanzania. *Mineral. Mag.* **2011**, *75*, 2801–2810. [CrossRef]
43. Zaitsev, A.N.; Williams, C.T.; Wall, F.; Zolotarev, A.A. Evolution of chemical composition of pyrochlore group minerals from phoscorites and carbonatites of the Khibina alkaline massif. *Geol. Ore Depos.* **2012**, *54*, 503–515. [CrossRef]
44. Broom-Fendley, S.; Wall, F.; Brady, A.E.; Gunn, A.G.; Chenery, S.R.; Dawes, W. Carbonatite-hosted, late-stage apatite as a potential source of heavy rare earth elements? In Proceedings of the 12th SGA Biennial Meeting Mineral Deposits Research for a High-Tech World, Uppsala, Sweden, 12–15 August 2013; pp. 1694–1697.
45. Linnen, R.L.; Samson, I.M.; Williams-Jones, A.E.; Chakhmouradian, A.R. Geochemistry of the rare-earth element, Nb, Ta, Hf and Zr deposits. In *Treatise on Geochemistry*, 2nd ed.; Elsevier: Amsterdam, The Netherlands, 2014; pp. 543–568.

46. Zaitsev, A.N.; Terry Williams, C.; Jeffries, T.E.; Strekopytov, S.; Moutte, J.; Ivashchenkova, O.V.; Spratt, J.; Petrov, S.V.; Wall, F.; Seltmann, R.; et al. Rare earth elements in phoscorites and carbonatites of the Devonian Kola Alkaline Province, Russia: Examples from Kovdor, Khibina, Vuoriyarvi and Turiy Mys complexes. *Ore Geol. Rev.* **2014**, *61*, 204–225. [CrossRef]
47. Chakhmouradian, A.R.; Reguir, E.P.; Kressall, R.D.; Crozier, J.; Pisiak, L.K.; Sidhu, R.; Yang, P. Carbonatite-hosted niobium deposit at Aley, northern British Columbia (Canada): Mineralogy, geochemistry and petrogenesis. *Ore Geol. Rev.* **2015**, *64*, 642–666. [CrossRef]
48. Moore, M.; Chakhmouradian, A.; Mariano, A.; Sidhu, R. Evolution of rare-earth mineralization in the Bear Lodge carbonatite, Wyoming: Mineralogical and isotopic evidence. *Ore Geol. Rev.* **2015**, *64*, 499–521. [CrossRef]
49. Song, W.; Xu, C.; Chakhmouradian, A.R.; Kynicky, J.; Huang, K.; Zhang, Z. Carbonatites of Tarim (NW China): First evidence of crustal contamination in carbonatites from a large igneous province. *Lithos* **2017**, *282–283*, 1–9. [CrossRef]
50. Reedman, J.H. Resources of phosphate, niobium, iron and other elements in residual soils over the Sukulu carbonatite complex, southeastern Uganda. *Econ. Geol.* **1984**, *79*, 716–724. [CrossRef]
51. Lottermoser, B.G. Rare earth element mineralisation within the Mt. Weld carbonatite laterite, Western Australia. *Lithos* **1990**, *24*, 151–167. [CrossRef]
52. Richardson, D.G.; Birkett, T.C. Residual Carbonatite-associated Deposits. In *Geology of Canadian Mineral Deposit Types*; Eckstrand, O.R., Sinclair, W.D., Thorpe, R.I., Eds.; Geological Survey of Canada: Ottawa, ON, Canada, 1996; pp. 108–119.
53. Morbidelli, L.; Beccccaluva, L.; Brotzu, P.; Conte, A.; Garbarino, C.; Gomes, C.B.; Macccciotta, G.; Ruberti, E.; Scheibe, L.F.; Traversa, G. Petrological and geochemical studies of alkaline rocks from continental Brazil. 3. Fenitization of jacupirangite by carbonatite magmas from Jacupiranga. *Per. Mineral.* **1986**, *55*, 261–295.
54. Drüppel, K.; Hoefs, J.; Okrusch, M. Fenitizing Processes Induced by Ferrocarbonatite Magmatism at Swartbooisdrif, NW Namibia. *J. Petrol.* **2005**, *46*, 377–406. [CrossRef]
55. Le Bas, M.J. Fenites associated with carbonatites. *Can. Mineral.* **2008**, *46*, 915–932. [CrossRef]
56. Smith, M.P.; Henderson, P.; Campbell, L.S. Fractionation of the REE during hydrothermal processes: Constraints from the Bayan Obo Fe-REE-Nb deposit, Inner Mongolia, China. *Geochim. Cosmochim. Acta* **2000**, *64*, 3141–3160. [CrossRef]
57. Ruberti, E.; Enrich, G.E.R.; Gomes, C.B.; Comin-Chiaramonti, P. Hydrothermal REE fluorocarbonate mineralization at Barra do Itapirauã, a multiple stockwork carbonatite, southern Brazil. *Can. Mineral.* **2008**, *46*, 901–914. [CrossRef]
58. Doroshkevich, A.G.; Viladkar, S.G.; Ripp, G.S.; Burtseva, M.V. Hydrothermal mineralization in the Amba Dongar carbonatite complex, Gujarat, India. *Can. Mineral.* **2009**, *47*, 1105–1116. [CrossRef]
59. Deines, P. Stable isotope variations in carbonatites. In *Carbonatites: Genesis and Evolution*; Bell, K., Ed.; Unwin Hyman: London, UK, 1989; pp. 301–359.
60. Woolley, A.R. Igneous silicate rocks associated with carbonatites: Their diversity, relative abundances and implications for carbonatite genesis. *Per. Mineral.* **2003**, *72*, 9–17.
61. Nielsen, T.F.D. The petrology of a melilitolite, melteigite, carbonatite and syenite concentric dyke system, in the Gardiner complex, East Greenland. *Lithos* **1980**, *13*, 181–197. [CrossRef]
62. Nielsen, T.F.D.; Solovova, I.P.; Veksler, I.V. Parental melts of melilitolite and origin of alkaline carbonatite: Evidence from crystallized melt inclusions, Gardiner complex. *Contrib. Mineral. Petrol.* **1997**, *126*, 331–344. [CrossRef]
63. Upton, B.G.J.; Craven, J.A.; Kirstein, L.A. Crystallisation of melaaillikites of the Narsaq region, Gardar alkaline province, south Greenland and relationships to other aillikitic–carbonatitic associations in the province. *Lithos* **2006**, *92*, 300–319. [CrossRef]
64. Tappe, S.; Steenfelt, A.; Heaman, L.M.; Simonetti, A. The newly discovered Jurassic Tikiusaaq carbonatite-aillikite occurrence, West Greenland and some remarks on carbonatite kimberlite relationships. *Lithos* **2009**, *112S*, 385–399. [CrossRef]
65. Moore, K.R.; Wall, F.; Divaev, F.K.; Savatenkov, V.M. Mingling of carbonate and silicate magmas under turbulent flow conditions: Evidence from rock textures and mineral chemistry in sub-volcanic carbonatite dykes, Chagatai, Uzbekistan. *Lithos* **2009**, *110*, 65–82. [CrossRef]

66. Melgarejo, J.C.; Costanzo, A.; Bambi, A.C.J.M.; Gonçalves, A.O.; Neto, B.N. Subsolidus processes as a key factor on the distribution of Nb species in plutonic carbonatites: The Tchivira case, Angola. *Lithos* **2012**, *152*, 187–201. [CrossRef]
67. Bambi, A.J.M.; Costanzo, A.; Gonçalves, A.O.; Melgarejo Draper, J.C. Tracing chemical evolution of primary pyrochlore from plutonic to volcanic carbonatites: The role of F. *Mineral. Mag.* **2012**, *76*, 377–392. [CrossRef]
68. Bambi, A.C.J.M. Metalogenia de las carbonatitas en dominios plutónicos, subvolcánicos y volcánicos: Tchivira, Bonga y Catanda, Angola. Ph.D. Thesis, Universitat de Barcelona, Barcelona, Spain, November 2015.
69. Amores-Casals, S.; Gonçalves, A.O.; Melgarejo, J.C.; Martí, J. Nb and REE distribution at the Monte Verde carbonatite–alkaline–agpaitic complex (Angola). *Minerals* **2019**. under review.
70. Amores, S. Evolución metalogenética de complejos carbonatíticos en contexto hipoabisal y plutónico: Bonga y Monte Verde (Angola). Ph.D. Thesis, Universitat de Barcelona, Barcelona, Spain, September 2017.
71. Torró, L.; Villanova, C.; Castillo, M.; Campeny, M.; Gonçalves, A.O.; Melgarejo, J.C. Niobium and rare earth minerals from the Virulundo carbonatite, Namibe, Angola. *Mineral. Mag.* **2012**, *76*, 393–409.
72. Campeny, M.; Mangas, J.; Melgarejo, J.C.; Bambi, A.C.J.M.; Alfonso, P.; Gernon, T.; Manuel, J. The Catanda extrusive carbonatites (Kwanza Sul, Angola): An example of explosive carbonatitic volcanism. *B Volcanol.* **2014**, *76*, 818–833. [CrossRef]
73. Lapido-Loureiro, F.E.V.; Sarmento Bravo, M. Sobre duas jazidas de fluorite em Angola. *Boletim do Instituto de Investigação Científica de Angola* **1966**, *3*, 251–256.
74. Beleque, A.R.C. Minerais de ETR no complexo carbonatítico de Bailundo (Mungo, Angola): Ocorrência, composição e significado económico. Master's Thesis, Departamento de Geologia, Faculdade de Ciências, Universidade de Lisboa, Lisboa, Portugal, 2010.
75. Lapido-Loureiro, F.E.V. Carbonatitos de Angola. *Memórias e Trabalhos do Instituto Investigação Científica de Angola* **1973**, *11*, 1–242.
76. Zhang, Y.; Gu, X.; Peng, Y.; Zheng, L.; Zhang, Y.; Gao, H.; Dong, S. Geology and genesis of the Bonga carbonatite type niobium deposit, Angola. *Earth Sci. Front.* **2014**, *21*, 50–68.
77. Alberti, A.; Castorina, F.; Censi, P.; Comin-Chiaramonti, P.; Gomes, C.B. Geochemical characteristics of Cretaceous carbonatites from Angola. *J. Afr. Earth Sci.* **1999**, *29*, 735–759. [CrossRef]
78. Comin-Chiaramonti, P.; Barros Gomes, C.; Cundari, A.; Castorina, F.; Censi, P. A review of carbonatitic magmatism in the Paraná-Angola-Namibia (PAN) system. *Period. Mineral.* **2007**, *76*, 25–78.
79. Coltorti, M.; Alberti, A.; Beccaluva, L.; Dos Santos, A.B.; Mazzucchelli, M.; Morais, E.; Rivalenti, G.; Siena, F. The Tchivira-Bonga alkaline carbonatite complex (Angola): Petrological study and comparison with Brazilian analogues. *Eur. J. Mineral.* **1993**, *5*, 1001–1024. [CrossRef]
80. Castorina, F.; Censi, P.; Barbieri, M.; Comin-Chiaramonti, P.; Cundari, A.; Gomes, C.B.; Pardini, G. *Carbonatites from eastern Paraguay: A comparison with coeval carbonatites from Brazil and Angola*; Comin-Chiaramonti, P., Gomes, C.B., Eds.; Alkaline Magmatism, in Central-Eastern Paraguay; Relationships with Coeval Magmatism in Brazil; EDUSP: São Paulo, Brazil, 1996; pp. 231–248.
81. Pereira, E.; Rodrigues, J.; Reis, B. Synopsis of Lunda geology, NE Angola: Implications for diamond explorations. *Comum. Inst. Geol. Min.* **2003**, *90*, 189–212.
82. Robles-Cruz, S.E.; Escayola, M.; Jackson, S.; Galí, S.; Pervov, V.; Watangua, M.; Gonçalves, A.; Melgarejo, J.C. U-Pb SHRIMP geochronology of zircon from the Catoca kimberlite, Angola. Implication for diamond exploration. *Chem. Geol.* **2012**, *310–311*, 137–147. [CrossRef]
83. Castillo-Oliver, M.; Galí, S.; Melgarejo, J.C.; Griffin, W.L.; Belousova, E.; Pearson, N.J.; Watangua, M.; O'Reilly, S.Y. Trace-element geochemistry and U-Pb dating of perovskite in kimberlites of the Lunda Norte Province (NE Angola): Petrogenetic and tectonic implications. *Chem. Geol.* **2016**, *426*, 118–134. [CrossRef]
84. Issa Filho, A.; Dos Santos, A.B.R.M.D.; Riffel, B.F.; Lapido-Loureiro, F.E.V.; McReath, I. Aspects of the geology, petrology and chemistry of some Angolan carbonatites. *J. Geochem. Explor.* **1991**, *40*, 205–206. [CrossRef]
85. Giuliani, A.; Campeny, M.; Kamenetsky, V.; Alfonso, J.C.; Maas, R.; Melgarejo, J.C.; Kohn, B.P.; Matchan, E.L.; Mangas, J.; Gonçalves, A.O.; et al. Southwestern Africa on the burner: Pleistocene carbonatite volcanism linked to deep mantle upwelling in Angola. *Geology* **2017**, *45*, 971–974. [CrossRef]
86. Campeny, M. Caracterización del Vulcanismo Carbonatítico de Catanda. PhD Thesis, Universitat de Barcelona, Barcelona, Spain, November 2015.
87. Dunworth, E.; Bell, K. Melilitolites: A new scheme of classification. *Can. Mineral.* **1998**, *36*, 895–903.

88. Zheng, L.; Gu, X.; Zhang, Y. Pyrochlore chemistry from the Bonga carbonatite type Nb deposit, Huila Province, Angola: Implications for magmatic-processes of carbonatite. *Acta Geol. Sin.* **2014**, *2*, 487–488. [CrossRef]
89. Atencio, D.; Andrade, M.B.; Christy, A.G.; Gieré, R.; Kartashov, P.M. The pyrochlore supergroup of minerals: Nomenclature. *Can. Mineral.* **2010**, *48*, 673–698. [CrossRef]
90. Chakhmouradian, A.R.; Mitchell, R.H. Occurrence, alteration patterns and compositional variation of perovskite in kimberlites. *Can Miner.* **2000**, *38*, 975–994. [CrossRef]
91. Bayliss, P.; Mazzi, F.; Munno, R.; White, T.J. Mineral nomenclature: Zirconolite. *Mineral. Mag.* **1989**, *53*, 565–569. [CrossRef]
92. Bulakh, A.G.; Nesterov, A.R.; Williams, C.T.; Anisimov, I.S. Zirkelite from the Sebl'yavr carbonatite complex, Kola Peninsula, Russia: An X-ray and electron microprobe study of a partially metamict mineral. *Mineral. Mag.* **1998**, *62*, 837–846. [CrossRef]
93. Kesson, S.E.; Sinclair, W.J.; Ringwood, A.E. Solid solution limits in SYNROC zirconolite. *Nucl. Chem. Waste Manage.* **1983**, *4*, 259–265.
94. Gieré, R.; Williams, C.T.; Lumpkin, G.R. Chemical characteristics of natural zirconolite. *Schweiz. Mineral. Petrogr. Mitt.* **1998**, *78*, 433–459.
95. Ivanyuk, G.Y.; Konopleva, N.G.; Yakovenchuk, V.N.; Pakhomovsky, Y.A.; Panikorovskii, T.L.; Kalashnikov, A.O.; Bocharov, V.N.; Bazai, A.A.; Mikhailova, J.A.; Gorianov, P.M. Three-D Mineralogical Mapping of the Kovdor Phoscorite-Carbonatite Complex, NW Russia: III. Pyrochlore Supergroup Minerals. *Minerals* **2018**, *8*, 277. [CrossRef]
96. Williams, C.T. The occurrence of niobian zirconolite, pyrochlore and baddeleyite in the Kovdor carbonatite complex, Kola Peninsula, Russia. *Mineral. Mag.* **1996**, *60*, 639–646. [CrossRef]
97. Bulakh, A.G.; Nesterov, A.R.; Anastasenko, G.F.; Anisimov, I.S. Crystal morphology and intergrowths of calzirtite $Ca_2Zr_5TiO_{16}$, zirkelite $(Ti,Ca,Zr)O_{2-x}$, zirconolite $CaZrTi_2O_7$ in phoscorites and carbonatites of the Kola Peninsula (Russia). *N. Jb. Miner. Mh.* **1999**, *1*, 11–20.
98. Rubin, J.N.; Henry, C.D.; Price, J.G. The mobility of zirconium and other "immobile" elements during hydrothermal alteration. *Chem. Geol.* **1993**, *110*, 29–47. [CrossRef]
99. Della Ventura, G.; Williams, T.C.; Raudsepp, M.; Bellatreccia, F.; Caprilli, E.; Giordano, G. Perrierite-(Ce) and zirconolite from a syenitic ejectum of the Roccamonfina volcano (Latium, Italy): Implications for the mobility of Zr, Ti and REE in volcanic environments. *N. Jb. Miner. Mh.* **2001**, *9*, 385–402.
100. Bellatreccia, F.; Della Ventura, G.; Williams, C.T.; Lumpkin, G.R.; Smith, K.L.; Colella, M. Non-metamict zirconolite polytypes from the feldspathoid-bearing alkali-syenitic ejecta of the Vico volcanic complex (Latium, Italy). *Eur. J. Mineral.* **2002**, *14*, 809–820. [CrossRef]
101. Castellano, A.; Melgarejo, J.C.; Bambi, A.C.J.M.; Gonçalves, A.O.; Alfonso, P. Nb and REE at the Bailundo carbonatite, Angola. In *Let's Talk Ore Deposits*; Barra, F., Ed.; Universidad Católica del Norte: Antofagasta, Chile, 2011; pp. 675–677.
102. Barbosa, E.S.R.; Brod, J.A.; Junqueira-Brod, T.C.; Dantas, E.L.; Cordeiro, P.F.O.; Gomide, C.S. Bebedourite from its type area (Salitre I complex): A key petrogenetic series in the Late-Cretaceous Alto Paranaiba kamafugite-carbonatite-phoscorite association, Central Brazil. *Lithos* **2012**, *144*, 56–72. [CrossRef]
103. Palmieri, M. Modelo geológico e avaliação de recursos minerais do depósito de nióbio do Morro do Padre, Complexo alcalino carbonatítico de Catalão II, GO. Master's Thesis, University of Brasília, Brasília, Brazil, 2011.
104. Cordeiro, P.F.O.; Brod, J.A.; Palmieri, M.; de Oliveira, C.G.; Barbosa, E.S.R.; Santos, R.V.; Gaspar, J.C.; Assis, L.C. The Catalão I niobium deposit, central Brazil: Resources, geology and pyrochlore chemistry. *Ore Geol. Rev.* **2011**, *41*, 112–121. [CrossRef]
105. Blake, S. Volcanism and dynamics of open magma chambers. *Nature* **1981**, *289*, 783–785. [CrossRef]
106. Blake, S. Volatile oversaturation during the evolution of silicic magma chambers as an eruption trigger. *J. Geoph. Res.* **1984**, *89*, 8237–8244.
107. Folch, A.; Martí, J. The generation of overpressure in felsic magma chambers by replenishment. *Earth Planet. Sci. Lett.* **1998**, *163*, 301–314. [CrossRef]
108. Lottermoser, B.G.; England, B.M. Compositional variation in pyrochlores from the Mt. Weld Carbonatite laterite, Western Australia. *Miner. Petrol.* **1988**, *38*, 37–51. [CrossRef]

109. Laval, M.; Johan, V.; Tourlière, B. La carbonatite de Mabounie: Exemple de formation d'un gîte residuel à pyrochlore. *Chronique de la recherché minière* **1988**, *491*, 125–136.
110. Nasraoui, M.; Bilal, E. Pyrochlores from the Lueshe carbonatite complex (Democratic Republic of Congo): A geochemical record of different alteration stages. *J. Asian Earth Sci.* **2000**, *18*, 217–251. [CrossRef]
111. Mitchel, R.H. Primary and secondary niobium mineral deposits associated with carbonatites. *Ore Geol. Rev.* **2015**, *64*, 626–641. [CrossRef]
112. Zheng, L.; Zhang, Y.; Gu, X.; Gao, H.; He, G.; Dong, S. Lithogeochemistry and carbon-oxygen isotopic study of mineralized carbonatite from the Bonga niobium deposit, Angola. *Acta Petrol. Sin.* **2017**, *33*, 2633–2647.
113. Broom-Fendley, S.; Styles, M.T.; Appleton, D.; Gunn, G.; Wall, F. Evidence for dissolution-reprecipitation of apatite and preferential LREE mobility in carbonatite-derived late-stage hydrothermal processes. *Am. Mineral.* **2016**, *101*, 596–611. [CrossRef]
114. Lottermoser, B.G. Churchite from the Mt Weld carbonatite laterite, Western Australia. *Mineral. Mag.* **1987**, *51*, 468–469. [CrossRef]
115. Morgavi, D.; Arienzo, I.; Montagna, C.; Perugini, D.; Dingwell, D.B. Magma mixing: History and dynamics of an eruption trigger. In *Volcanic Unrest*; Gottsmann, J., Neuberg, J., Scheu, B., Eds.; Advances in Volcanology; Springer: Cham, Switzerland, 2017. [CrossRef]